UNIVERSIDADE DA BEIRA INTERIOR
Ciências da Saúde

Detection of biometals signature of brain tissues by X-ray fluorescence

Patrícia Gonçalves D'Amil

Dissertação para obtenção do Grau de Mestre em
Ciências Biomédicas
(2º ciclo de estudos)

Orientador: Prof. Doutor Jorge Maia
Co-orientador: Doutora Ana Clara Cristóvão

Covilhã, 2 Outubro de 2015

O conteúdo do presente trabalho é da exclusiva responsabilidade da autora:

_____

(Patrícia Gonçalves D'Amil)

Agradecimentos

Queria agradecer, em primeiro lugar, ao meu orientador, Professor Doutor Jorge Manuel Maia Pereira, do Departamento de Física da Universidade da Beira Interior e do LIP-Coimbra, Laboratório de Instrumentação e Física Experimental de Partículas, pela sugestão do tema, pelo apoio ao longo deste ano e acima de tudo pelos conhecimentos que me foi passando à medida que o projecto avançava. Quero também estender este agradecimento à Doutora Ana Clara Braz Cristóvão, do CICS-Centro de Investigação em Ciências da Saúde da Universidade da Beira Interior pelo apoio, essencial, na realização deste projecto.

Um agradecimento especial ao Professor Doutor José António Carvalho Paixão, coordenador do TAIL-UC (*Trace Analysis and Imaging Laboratory* da Universidade de Coimbra) onde parte deste trabalho foi realizado, e ao Doutor Pedro Sidónio, responsável pelo laboratório, pela disponibilidade e apoio técnico ao espectrómetro de fluorescência de raios X por energia dispersiva.

Ao LIP-Coimbra por me terem recebido e por todo o apoio prestado ao longo deste trabalho. Em particular quer agradecer ao técnico Américo Pereira e ao Mestre Alexandre Trindade por todo o seu apoio.

Ainda do LIP-Coimbra quero agradecer à Mariana Martins, ao Pedro Crispim e ao Miguel Moita por me terem recebido tão bem e por toda a ajuda que me deram.

Ao Marco Pinto por me ter ajudado na chegada a Coimbra e por não ter deixado de o fazer mesmo à distância.

À Patrícia Lindeza, por me ter ajudado tanto nesta recta final. Pela preocupação, pela disponibilidade e pelo *timing* tão importante e pela força.

Às pessoas que tornaram melhor a minha estadia em Coimbra, Mónica Santos, Jéssica Mesquita, Marco Rodrigues e Luís Aurélio. Muito obrigada! É por vocês que agora, Coimbra é saudade.

À minha família, aos meus pequenos Rúben e Diana, à minha mãe e ao meu pai. Sem vocês nada disto teria sido possível. E claro, à Elizabeth, Paulo, Filipa por estarem sempre disponíveis e por me ajudarem tanto.

À Rita Carneiro por estar sempre presente, pela ajuda, pela compreensão, pela disponibilidade a qualquer hora.

Finalmente, ao João Ferreira por estar sempre ao meu lado, nos melhores e nos piores momentos. Por ter tido a paciência e a compreensão necessárias para me acompanhar ao longo de todo este percurso.

Ao meu mais recente companheiro de trabalho, Paulo Fura, por ter acompanhado esta fase final ajudando-me a manter-me focada.

A todos, muito obrigada!

Resumo

A espectrometria de fluorescência de raios X por energia dispersiva é uma técnica que permite a identificação de elementos atómicos em amostras sem interferir com a estrutura das mesmas. Inicialmente a amostra é excitada com um feixe primário de raios X que promove a emissão de raios X de fluorescência, característicos dos elementos atómicos constituintes da amostra. De seguida, e baseando-se na energia dos raios X de fluorescência característicos emitidos, o espectrómetro de raios X monta um espectro de energia onde a cada elemento atómico detetado corresponde um pico com energia característica, cuja área é uma medida indirecta da concentração do elemento na amostra.

A doença de Parkinson é a segunda doença neurodegenerativa mais comum em todo o mundo, a seguir à doença de Alzheimer, afectando cerca de 0.3% da população dos países industrializados. Esta patologia caracteriza-se por causar tremor, rigidez, dificuldade em iniciar movimentos e postura instável. A causa desta condição é a degeneração de neurónios dopaminérgicos na *substantia nigra* que, em condições normais, são responsáveis pela produção de dopamina e libertá-la no *striatum*, ajudando no controlo dos músculos envolvidos nos movimentos e na coordenação motora.

Na literatura têm sido documentadas algumas alterações na concentração de elementos atómicos em amostras de cérebros com doença de Parkinson. Deste modo, propôs-se realizar medições da intensidade de raios X de fluorescência característicos em amostras nas quais esta patologia foi induzida por Paraquat e em amostras controlo quer na *substantia nigra* quer no *striatum*.

O objectivo deste trabalho consistiu na optimização das condições de operação do espectrómetro de fluorescência de raios X por energia dispersiva no intuito de numa fase posterior identificar possíveis alterações na concentração dos elementos medidos no modelo de Parkinson utilizado.

Ao nível dos resultados, a optimização dos parâmetros do equipamento no sentido de obtermos as melhores condições de identificação e medição da concentração dos elementos foi conseguida. No que diz respeito à alteração dos elementos medidos nos dois grupos, o controlo e o tratado com paraquato, as diferenças não foram, no geral, estatisticamente significativas excepto no caso do cobre, que se mostrou aumentado no *striatum* (≈15%).

Palavras-chave

Doença de Parkinson, Fluorescência, Raios-X, Paraquat, Metais, Ferro, Cobre, Zinco.

Resumo Alargado

A espectrometria de fluorescência de raios X por energia dispersiva é uma técnica que permite a identificação de elementos atómicos em amostras sem interferir com a estrutura das mesmas. Inicialmente a amostra é excitada com um feixe primário de raios X que promove a emissão de raios X de fluorescência, característicos dos elementos atómicos constituintes da amostra. De seguida, e baseando-se na energia dos raios X de fluorescência característicos emitidos, o espectrómetro de raios X monta um espectro de energia onde a cada elemento atómico detetado corresponde um pico com energia característica, cuja área é uma medida indirecta da concentração do elemento na amostra.

A doença de Parkinson é uma doença neurodegenerativa, a segunda mais comum em todo o mundo e afecta cada vez mais pessoas, sendo que, nos países industrializados a percentagem de doentes é de cerca de 0.3%. Esta condição tem como consequências tremor, rigidez, dificuldade em iniciar movimentos e instabilidade em termos de postura.

Esta patologia caracteriza-se pela degeneração dos neurónios dopaminérgicos, localizados na *substantia nigra*. Estes, em condições normais são responsáveis pela produção de dopamina e consequente libertação no *striatum*. Em conjunto estas estruturas são responsáveis pelo movimento e coordenação motora.

Há evidências que demonstram que a degeneração celular na doença de Parkinson pode ser despoletada pelo stress oxidativo. O organismo no geral tem mecanismos de defesa contra esta condição mas aparentemente o cérebro é mais sensível aos danos do que os outros órgãos. As células dopaminérgias sofrem, especialmente, com esta condição pois durante a produção de dopamina ocorre também a formação de espécies reactivas de oxigénio, responsáveis pelo aumento do stress oxidativo.

A manutenção da homeostase dos metais no cérebro é de extrema importância. Estes, quando presentes em quantidades normais são indespensáveis para o normal funcionamento do cérebro mas podem tornar-se perigosos quando não estão em equilibrio. Por exemplo, o ferro tem funções crucias em processos metabólicos como a respiração mitocondrial, síntese de proteínas e biossíntese de neurotransmisores. Mas, quando desregulado, como metal de transição, pode participar em reações que aumentam consideravelmente a quantidade de radicias livres. O mesmo se passa com o cobre. Este tem um papel muito importante pois funciona como co-factor da enzima anti-oxidante superóxido dismutase. Mas, quando aumentado, o cobre tem a capacidade de participar em reações que promovem a formação de radicias livres. No caso do zinco, este tem uma função importante no sistema imunitário e, como é um metal inerte, não participa em reações que originam radicais livres.

O objectivo deste trabalho consistiu na optimização das condições de operação do espectrómetro de fluorescência de raios X por energia dispersiva de modo a conseguir identificar alguns elementos atómicos para posteriormente fazer a caracterização em termos dos elementos atómicos de um grupo de roedores aos quais foi induzida doença de Parkinson e compará-los com um grupo normal. Para a indução da doença de Parkinson foi utlizado um modelo que reproduz muitas das características da patologia, como a degeneração de neurónios dopaminérgicos e que consiste na injecção intraperonial de um composto, o paraquato.

A cada indíviduo de cada um dos grupos foram retiradas duas amostras de tecido cerebral, uma da *substantia nigra* e uma do *striatum*. Ambas foram analisadas utilizando condições definidas após a optimização dos parâmetros espectrómetro de fluorescência de raios X e depois procedeu-se ao tratamento dos dados de forma a tentar estabelecer uma comparação entre os dois grupos. Para cada uma das regiões do cérebro foram utilizados três filtros de raios X que nos permitiram analisar determinados elementos atómicos. O filtro para o cloro, que permitiu analisar fósforo, enxofre, cloro, potássio e cálcio; o filtro para o crómio que permitiu analisar todos os elementos referidos e o ferro; e o filtro para o mapeamento de chumbo que possibilitou a análise de ferro, cobre e zinco.

Em termos de resultados, podemos afirmar que a optimização das condições de operação do espectrómetro de fluorescência de raios X foi conseguida, uma vez que conseguimos medir e analisar vários elementos atómicos importantes em ambas as regiões do cérebro. No que diz respeito à comparação entre os dois grupos, apenas a medição de um dos elementos (cobre) no *striatum* foi considerada estatisticamente significativa. Apesar disso, pode observar-se uma tendência em alguns dos elementos como por exemplo, o cloro aumenta sempre, o cálcio diminui, o cobre aumenta e o zinco diminui. No caso do ferro os resultados não foram significativos uma vez que este aumenta com filtro para mapeamento de chumbo e diminui com o filtro para o crómio. As variações nos elementos mais leves, fósforo, enxofre e potássio não seguem uma tendência.

Abstract

Energy dispersive X-ray fluorescence (EDXRF) spectrometry is a technique that allows the identification of atomic elements in samples without interfering with its structure. Firstly, the sample is excited with a primary X-ray beam that causes the emission of fluorescence X-rays, characteristic from the atomic elements in the sample. After this, and based on the energy of the fluorescence X-rays, the spectrometer is able to create a spectrum of energy wherein each atomic element detected has a characteristic peak with its characteristic energy, whose area is an indirect measure of the concentration of the element in the sample.

Parkinson's disease is the second more common neurodegenerative pathology in all world, affecting around 0.3% of industrialized countries population. This disease is characterized by resting tremor, rigidity, difficulty in initiating movement and postural instability. The cause of this condition is the degeneration of dopaminergic neurons in *substantia nigra* which, in normal conditions, are responsible for the production of dopamine and release it in *striatum*, helping in the control of muscles involved in movement and co-ordination.

In the literature have been documented some atomic element changes in brain samples with Parkinson's disease. Thus, we propose to perform X-ray fluorescence intensity measurements in tissue samples in which this pathology was induced by Paraquat and control tissue samples in both *substantia nigra* and *striatum*.

The purpose of this study was to optimize the conditions of operation of the X-ray fluorescence spectrometer in order to, *a posteriori*, identify possible alterations in the concentration of the atomic elements measured in the Parkinson model used.

In terms of results, optimization of spectrometer parameters was achieved. Relatively to the distinction of the two groups, the differences were not in general statistically significant except for the copper, which showed an increased content in *striatum* (≈15%).

Keywords

Parkinson's disease, X-ray, Fluorescence, Paraquat, metal, iron, copper and zinc.

Index

List of figures

Chapter 1

Chapter 2

Chapter 3

List of Tables

Chapter 1

Chapter 2

List of Acronyms

6-OHDA	6-hydroxydopamine
α-syn	α-synuclein
BBB	Blood Brain Barrier
CNS	Central Nervous System
DMT	Divalent Metal Transporter
EDS	Energy Dispersive X-Ray Spectroscopy
EDXRF	Energy Dispersive X-Ray Fluorescence
EELS	Electron Energy Loss Spectroscopy
EPMA	Electron Photon Micro Analysis
FWHM	Full Width at Half Maximum
GSH	Glutathione
ICP-MS	Inductively Coupled Plasma Mass Spectrometry
LA-ICP-MS	Laser Ablation Inductively Coupled Plasma Mass Spectrometry
LB	Lewy Bodies
LIP	Labile Iron Pool
MAO	Monoamine Oxidase
MCA	Multi-Channel Analyzer
MPTP	N-metyl-4-phenyl-1,2,3,6-tetrahydroxypyridine
MRI	Magnetic Resonance Imaging
OH	Hydroxyl Radical
PD	Parkinson's Disease
PIXE	Particle Induced X-Ray Emission
PQ	Paraquat
ROI	Region of Interest
ROS	Reactive Oxygen Species
SEM	Scanning Electron Microscopy
SIMS	Secondary Ion Mass Spectrometry
SN	*Substantia Nigra*
SNpc	*Substantia Nigra pars compacta*
SOD	Superoxide Dismutase
ST	*Striatum*
TEM	Transmission Electron Microscopy
XFM	X-Ray Fluorescence Microscopy
XRF	X-Ray Fluorescence

Chapter 1 - Introduction

1.1. Measurement of Metals in Biologic Tissues

1.1.1. Analytical techniques to measure metals

There are evidences that link the deregulation of metal homeostasis to the neuropathology of neurodegenerative disorders [1-6]. This section presents some of the techniques that can be used to measure metals in biological tissues.

There are some traditional methods to obtain information about samples elemental composition as atomic absorption spectrometry and inductively coupled plasma mass spectrometry (ICP - MS) [7]. Atomic absorption spectrometry is a method for quantitative determination of chemical elements using the absorption of light by free atoms of the sample in the gaseous state (atomized samples). In this technique the concentration of a particular element in the sample is analyzed. ICP–MS is a type of mass spectrometry which is capable of detecting metals in low concentrations. This technique uses ionized samples, so, as atomic absorption spectrometry, although afford high sensitivity, the localization of the elements in the samples is lost [8].

For the location of the elements staining methods can be used. The disadvantage of these methods is the low sensitivity to small concentrations of bio metals and, furthermore, the coloration is only sensitive to free ions [7]. Next, in Table 1, these techniques and their advantages and disadvantages are summarized.

Table 1.1. – Example of some traditional methods to measure metals and their advantages and disadvantages.

Technique	Advantage	Disadvantage
Atomic absorption spectrometry	High Sensitivity	Homogenized samples (loss of location)
ICP-MS	High Sensitivity	Homogenized samples (loss of location)
Staining Methods	Location of the elements	Low sensitivity (only free ions)

There are also some other techniques to measure metals, which have a high spatial resolution and sensitivity, to measure metals in tissues providing important information on cellular mechanisms of neurodegenerative diseases. Among these techniques are included synchrotron

X-ray fluorescence microscopy (XFM), particle induced X-ray emission (PIXE), electron energy loss spectroscopy (EELS) and secondary ion mass spectrometry (SIMS) [7].

X-ray fluorescence microscopy (XFM) is a technique that uses a very thin X-ray beam (provided from synchrotron) to excite samples inducing the emission of fluorescence X-rays that allow the identification of the elements present thereon [9, 10]. This technique has a high sensitivity and allows submicron spatial resolution [11].

Particle induced X-ray emission (PIXE) is a technique that uses a beam of accelerated particles to analyze a sample. Then the sample emits characteristic fluorescence X-rays that are detected and used to discriminate and quantify the presence of the different elements in the specimen [12]. This method it's similar to XFM, excepted from the constitution of the beam, particles instead of X-rays [7].

Electron energy loss spectroscopy (EELS) utilizes an electron beam of known kinetic energy and measures the energy lost by the electron through inelastic scattering with the sample [7]. This technique also has an high sensitivity [13].

Secondary ion mass spectrometry (SIMS) imaging uses an ion beam to remove ions from the sample. Then, the secondary ions (removed from the samples) are then measured and the image is made. As this technique requires an high vacuum environment these experiments could be more difficult to perform [7]. It is the most popular ion mass spectrometry technique. With the use of a thin and focused beam of ions, it has the highest spatial resolution [14]. A resume of all these techniques is represented in table 2 below.

Table 1.2. – Resume of some other techniques used to measure metals and their main characteristics.

Technique	Source of excitation	Characteristics
XFM	X-ray beam (synchrotron)	Submicron Resolution
PIXE	Protons	Submicron Resolution
EELS	Electron Beam	High Sensitivity
SIMS	Ion Beam	Highest Spatial Resolution

1.1.2. The X-Ray Fluorescence (XRF) Spectrometry

X-rays form part of the electromagnetic wave spectrum which includes radio waves, microwaves, infrared and visible radiation and gamma rays. The electromagnetic spectrum is represented in figure 1 below.

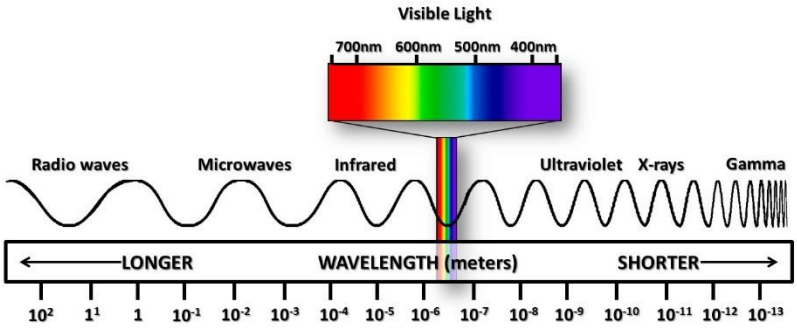

Figure 1.1 - Electromagnetic spectrum [15].

X-rays were accidentally discovered by W. K. Röntgen while researching discharge tubes in 1895. Röntgen found that a screen used to cover a discharge tube glowed. He observed that by placing an object between the discharge tube and screen, a shadow of that object would be revealed on the screen. It was then recognized that this discovery might be used to look into the human body and other materials [16].

W. K. Röntgen discovered that X-rays have the ability to penetrate matter and that the penetrating X-rays are absorbed by matter, depending on which elements make up the matter. The larger the atomic number of the elements making up the substance, the larger will be the absorption effect [17]. This ability to penetrate tissue is due to, as can be seen in figure 1, X-rays short wavelength and high energy. The wavelength of these rays is between 0.01 and 10 nm corresponding to a range of energy between 100 eV and 100 keV [18].

Absorption of X-rays by a sample depends not only on the atomic number of each element in the substance but on the wavelength of the irradiating X-rays, the thickness and the elemental composition of the substance [17].

When an X-ray of certain energy hits a sample, the atoms of the sample are ionized and stay in a state of excitation. In the desexcitation to the fundamental sate they emit characteristic X-rays, called fluorescence X-rays [16]. These emitted X-rays have energies (wavelength) characteristic of each element in the substance. By examining the X-ray energy, the properties of an unknown sample can be analyzed and the sample identified [18, 19].

The energy that a given electron has is unique and depends, among another variables, in which of the atom shells the electron is. The electrons on K-shell have higher absolute value of energy than those in L and so on. The value of this energy is typical from the atom [18].

Recalling Bohr's postulate that radiations are emitted only as a result of transfer of electrons between energy levels, it is therefore necessary to eject an electron from the atom in order to initiate the process for the emission of a radiation that is characteristic of the atom. For example, in X-ray fluorescence spectrometry, the ejection of K-shell electrons from atoms to generate the K spectral series requires that the incident photons energy overcome the binding energy binding of those electrons, the same to the other shells (L, M, N, etc). Thus, binding energies are also referred to as critical excitation energies, since they set the minimal energy that must be equaled or exceeded in order to eject electrons from atoms, leaving the latter in an unstable or ionized state necessary to initiate the process that leads to the emission of characteristic X-rays [18]. Fluorescent X-rays are created when a substance, irradiated by primary X-rays, gives off secondary X-rays with energy that is characteristic of a certain element [16, 17]. This effect is illustrated below in the figure 1.2.

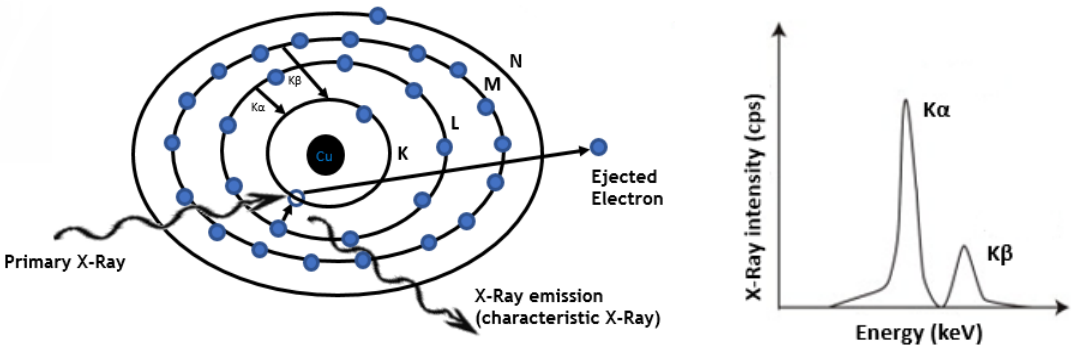

Figure 1.2. – Formation of fluorescence X-rays. Image adapted from SEA6000VX Operation Manual, Hitachi High-Tech Science Corporation, 2013 [17].

If an electron from the L-shell drops into the K-shell, a designed Kα X-ray is emitted. If an electron from the M-shell or from the N-shell drops into the K-shell, a K$_\beta$ X-ray is emitted. If the ejected electron belongs to L-shell, some transitions from M and N are, respectively, Lα and L$_\beta$ [17].

Taking this in consideration, X-ray fluorescence requires that samples to be irradiated by highly energetic photons. The energy source for irradiating specimens in most commercial X-ray fluorescence spectrometers is the polychromatic primary beam emanating from X-ray tubes [18].

To achieve the emanation of X-rays from an X-ray tube its necessary a tungsten filament (cathode) to be the source of electrons. These electrons are accelerated towards and focused on a metallic target (anode) by the application of a high voltage between the two electrodes

[18]. The incident electrons can interact by two different means producing a continuous X-ray spectrum (*Bremsstrahlung* radiation) or the characteristic fluorescence X-rays of the target element. These two phenomena are represented in figure 1.3 below [18]. In most XRF systems the beam of X-rays incident on the sample is produced with a vacuum tube and created by bombarding a target (such as Rh, W, Cu, or Mo) with highly accelerated electrons. As shown in Figure 1.3., as the electrons penetrate the target atoms, they may have their direction changed as they pass near the nucleus of the atoms causing a sudden deceleration and loss of kinetic energy. In this loss of kinetic energy the electron may emit an X-ray with energy related to the amount of energy lost. As a result a broad spectrum of X-ray energies, known as a *Bremsstrahlung* continuum, is emitted [18].

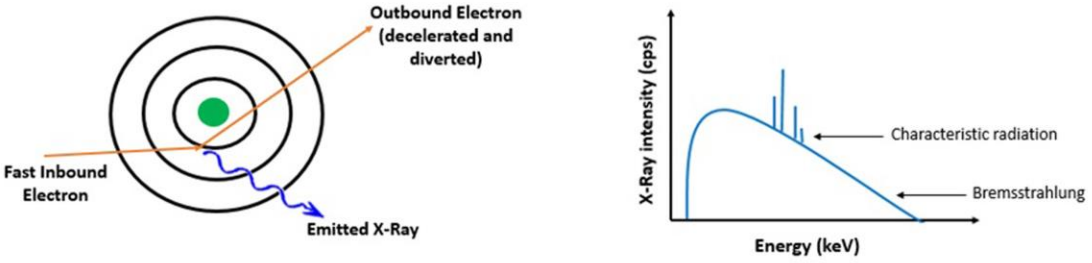

Figure 1.3 – *Bremsstrahlung* and characteristic radiation [20].

This continuum can be adjusted by tube high voltage settings, beam filtering and secondary targets to allow one to focus on detection of specific elements within the sample. The collision of the accelerated electrons with the target atoms also causes emission of characteristic fluorescence X-rays [18].

To produce fluorescence X-rays from a sample two processes have to occur, excitation and emission. First, a high energy beam is generated and it's the excitation source. Then, samples are irradiated and characteristic fluorescence X-rays of the elements presented are emitted [18].

As has been stated above, there are a set of techniques that can be used to measure metals. An example is laser ablation inductively coupled plasma mass spectrometry (LA-ICP-MS), as has also been explained before. XRF advantage when compared to this technique is that no sample preparation is required, and multiple atomic elements can be identified and measured. Additionally is nondestructive, so samples can be used for other purposes following the XRF analysis [4, 21]. Another example are the histochemical methods. Each one employs a different chemistry, and so they can't be combined or used sequentially on the same tissue section [4].

Unlike conventional histology sections, XRF samples retain metals because they do not have to be dehydrated or embedded, and after nondestructive XRF mapping, the same sample can be processed for histology or immunohistochemistry. XRF is the only way to nondestructively and simultaneously visualize multiple metals in the same section to estimate the effect of therapeutic drugs on brain metals [10, 22].

Ethically, this technique is also advantageous because we can analyze various elements just using a sample instead of using a different one to identify each element, as there are techniques that can identify only one element.

XRF serves as an alternative method with sensitivity and spatial resolution sufficient to reveal the distribution of metals in cells and brain tissues. This technique has unique capabilities for analyzing the distribution of metal ions in the context of metal induced neurotoxicity [23].

As shown in Figure 1.4 a), when an X-ray is irradiated into element A, fluorescent X-ray A is generated. When irradiated into element B, fluorescent X-ray B is generated [17].

When only the element A or B is excited, only the fluorescent X-ray A or B is irradiated but if a material with both A and B elements is irradiated both the A and B X-rays are generated, as is represented in Figure 1.4 b) [17].

The energies are separated and measured individually. When the concentrations of A and B components inside the material are changed, the intensity of A and B change as well [17].

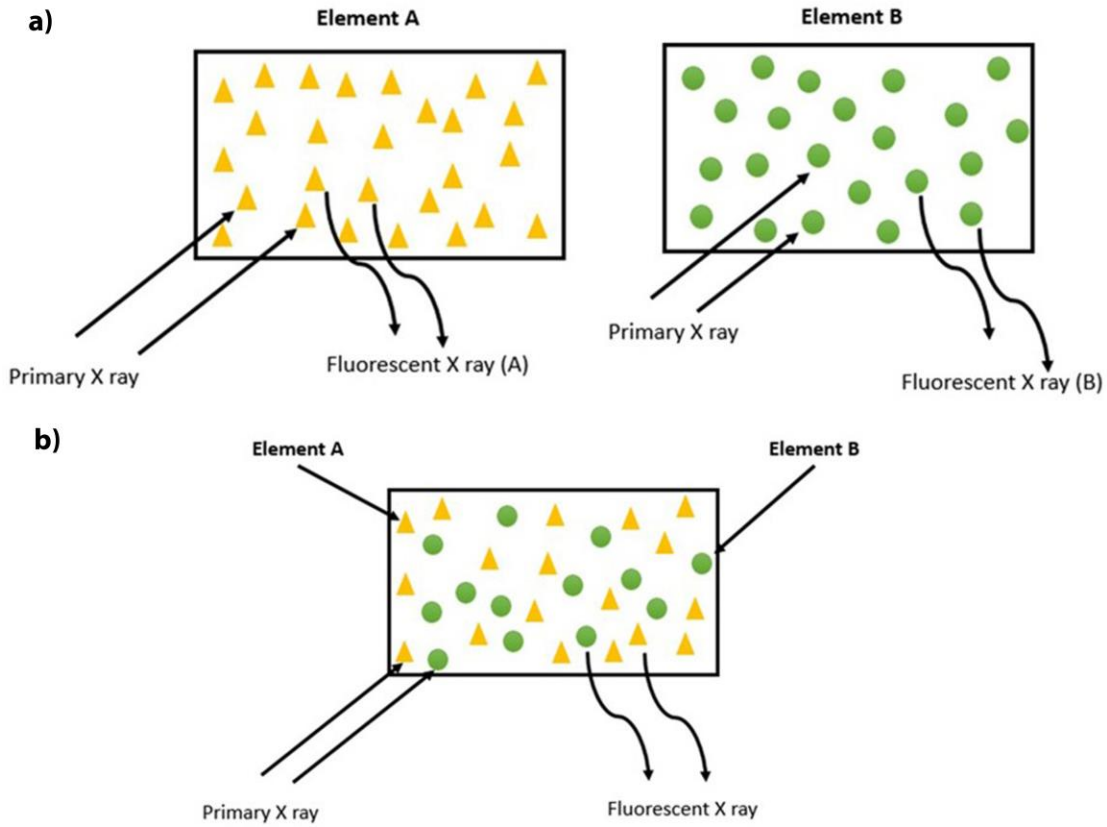

Figure 1.4. – a) Emission of fluorescence, characteristic from a single element sample, b) fluorescence emission in a multi element sample. Image adapted from SEA6000VX Operation Manual, Hitachi High-Tech Science Corporation, 2013 [17].

1.2. Parkinson Disease

1.2.1. General Considerations

Parkinson's disease (PD) is the second most common neurodegenerative disorder after Alzheimer disease, with prevalence in industrialized countries of approximately 0.3% of the population. This rises with age from 1% in those over 60 years of age to 4% of the population over 80, illustrating the effect of aging [24].

In terms of clinical features of PD, these include resting tremor, rigidity, difficulty in initiating movement and postural instability [25, 26]. Other motor features include gait and posture changes that manifest as festination (rapid shuffling steps with a forward-flexed posture when walking), speech and swallowing difficulties, a masklike facial expression and micrographia. Although this has been the classical textbook description of PD, more recently it has become recognized as a more complex illness encompassing both motor (referred above) and non-motor symptoms (NMS), such as depression, sleep disturbance, sensory abnormalities, autonomic dysfunction, and cognitive decline. NMS affect all patients with PD, the frequency of which increases with disease severity, with late stage patients exhibiting 6 to 10 NMS [24].

PD occurs as a consequence of the degeneration of dopamine producing neurons in a region of the midbrain called the *substantia nigra pars compacta* (SNpc) [22, 26-30]. In normal conditions dopaminergic neurons are responsible for the release of dopamine in striatum (ST), helping in the control of nerves and muscles involved in movement and co-ordination. Deficiency of dopamine in ST, caused by the death of dopaminergic neurons, is the main biochemical defect in PD [25]. Figure 1.5 represents the structures in a rodent brain which are affected by PD. SN, ST and their connection can been seen.

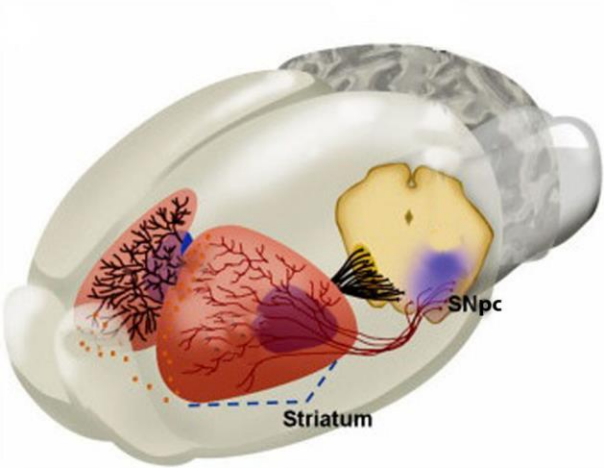

Figure 1.5 – Representation of the structures affected by Parkinson's disease in a rodent brain. Image adapted from Arias-Carrion *et al* [31].

1.2.2. Oxidative Stress

Many studies have shown that oxidative stress triggers a cascade of events which is responsible for neural cells death during PD [26, 28, 30, 32].

During cellular aerobic metabolism, reactive oxygen species (ROS) like superoxide ($O_2^{\bullet -}$), hydrogen peroxide (H_2O_2), hydroxyl radical ($OH^{\bullet}$) and peroxynitrite ($ONOO^-$) are generated. This molecules can be responsible for the damage of some cellular components such as proteins, nucleic acids and lipids leading to cellular degeneration. To protect the organism from these toxic agents there are detoxifying enzymes and antioxidants molecules. When there is either an increase production of ROS or a decrease in antioxidant defenses, there are toxic consequences for the cell. The level of oxidative damage caused by this condition stands as oxidative stress [28, 29].

Although the body in general has evolved several defense mechanisms to neutralize oxidative stress, the brain appears to be more susceptible to this damage than other organs [4, 28]. Dopaminergic neuronal cells of the SNpc are particularly vulnerable to such insult due to the ROS generated during dopamine (DA) metabolism [28].

1.2.3. Mitochondrial dysfunction

Mitochondria are responsible for generating 90% of the ATP necessary for all cellular functions, for detoxifying ROS production via mitochondrial respiration, for controlling the cellular redox state, and for regulating cytoplasmic calcium levels by acting as a major intracellular sink for this ion. Oxidative damage to the mitochondria might interfere with all of these functions [28].

Mitochondrial dysfunction is a basic problem associated with many neurodegenerative processes as well as normal aging [2, 4, 28] and it also constitutes a problem in PD [22, 33]. A proposed mechanism of neuronal death is the response to oxidative stress and abnormal calcium signaling causing mitochondrial dysfunction. Defects in mitochondrial respiration are responsible for the degeneration and death of neurons during the course of most, if not all, neurodegenerative disorders [2].

Thus, mitochondria play a key role in regulating cellular survival and death and are an important source of ROS within most mammalian cells such that mitochondria damage highly contributes to neurodegeneration [29].

1.2.4. α-Synuclein aggregation and formation of Lewy Bodies

Besides the dopaminergic neuronal lost, PD is characterized by the accumulation and aggregation of α-synuclein (α-syn) and the consequent formation of Lewy Bodies (LB) [3, 7, 25, 28, 29, 32, 34].

α-Syn is a small protein largely distributed throughout brain that can act as a negative regulator of DA synthesis. α-Syn aggregation is promoted by DA and its metabolites (iron, for example) and in this form (LB) it can't prevent DA synthesis [35]. As stated above, when in excess DA is responsible for the production of ROS [28].

There is a study confirming that elevated concentrations of DA are neurotoxic and that agents that can decrease DA are neuroprotectors. This study also links DA metabolism and its interaction with α-Syn to neurodegeneration explaining the susceptibility of dopaminergic neurons and, consequently SN, to neurodegeneration in PD [36].

1.3. Metals in Parkinson's disease

1.3.1. General

Essential metals are crucial for the maintenance of cell homeostasis. The neurobiology of metals is now growing in interest, since it has been linked to many neurodegenerative

diseases. Some metals appear to play an important role in oxidative stress, particularly in mitochondria, protein misfolding, and aggregation leading eventually to neurodegeneration [2-4, 7, 37, 38]. This is probably the result of a progressive deterioration of the metal regulatory systems and dysfunctional metal transport by brain barriers [39], which appear highly enhanced under various pathological conditions, causing increased oxidative stress [4] and favoring abnormal metal–protein interactions [2]. There is accumulating evidence that altered metal homeostasis may be involved in aggregation of intrinsically disordered proteins, for example, interacting on α-Syn structure and aggregation propensity [3, 7, 36, 40].

Transition metals play an important role in regulating neuronal activity within the synapses and they are essential for the biological functions of several metalloproteins such as Cu/Zn Superoxide Dismutase (SOD) and cytochrome c oxidase. Besides that, transition metals are required for many enzymatic activities, mitochondrial function, neurotransmission and memory [29].

Furthermore, as transition metals they have the ability to participate in redox reactions, making these elements responsible for ROS production and when in excess increasing oxidative stress [30].

As already stated above, metal ions are vital to ensure many cellular processes but their concentrations must be well regulated because abnormalities may lead to cell death and serious illness. There are a plethora of mechanisms responsible for that regulation so that the metal ion content is maintained in the required level and not in deficiency or excess. These mechanisms failure can lead to several disease state including neurodegenerative diseases [29].

1.3.2. Biometals as probes in Parkinson's disease

It has been observed that patients with PD tend to accumulate Fe in their nervous system [2, 3, 5, 7, 22, 25, 26, 28, 29, 41-44], suggesting a role for this transition metal in this disorder. Fe accumulation leads to excessive production of ROS, protein, DNA and phospholipid oxidation and, ultimately, to structural and functional damage [26, 29].

Iron is essential for normal neuronal functioning and is a crucial cofactor of multiple metabolic processes like oxygen transport, DNA and protein synthesis, mitochondrial respiration, myelination, dendrite development and neurotransmitters biosynthesis [41]. This metal is also an essential element for the normal development of cognitive functions [42]. It has been proved that iron deficiency in humans is responsible for a deterioration of cognitive functions [45].

Free iron is the major transition metal implicated in the participation on redox reactions *in vivo*. These reactions are responsible for the generation of ROS, which, in turn, cause oxidative stress [26].

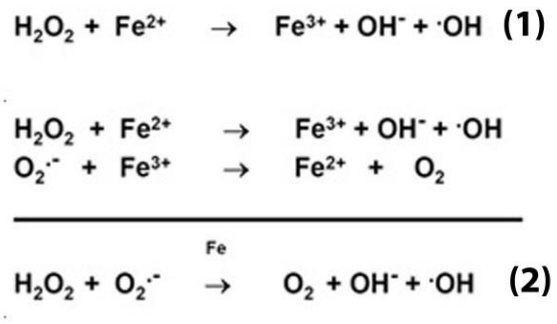

Figure 1.6 - Reactive oxygen species and redox cycling of iron. Fenton reaction is represented by equation (1) and describes the decomposition of hydrogen peroxide to the highly reactive hydroxyl radical, in the presence of ferrous iron. Iron-catalyzed Haber –Weiss reaction is represented by equation (2), also known as superoxide-driven Haber-Weiss reaction. Image adapted from Garcia Castineiras, 2010 [46].

Metals participate in redox reactions leading to the formation of superoxide and hydroxyl radicals, mostly via the Haber-Weiss reaction (number (2) in Figure 1.6 above) in which superoxide ($O_2^{\bullet -}$) promotes the reduction of ferric Fe^{3+} to ferrous Fe^{2+}. This reaction is followed by the Fenton reaction (number (1) in Figure 1.7. above) wherein ferrous Fe^{2+} and hydrogen peroxide (H_2O_2) react to generate ferric Fe^{3+}, hydroxide (OH^-), and the reactive hydroxyl radical ($OH^{\bullet}$). Cu^+ and Cu^{3+} ions may substitute for Fe^{2+} and Fe^{3+} ions in the Haber-Weiss reaction [2, 7, 22, 26, 28, 47].

Fenton reaction may be initiated by a small quantity of free iron, leading to the production of ROS which will cause damage to neurons. As it has been mentioned, Fe is a co-factor in the production of DA [27] and so it's not surprising that in SN high levels of iron could play an important role leading ultimately to the loss of dopaminergic neurons [26, 29]. This metal stimulates the auto-oxidation of dopaminergic neurons, liberating even more H_2O_2 and it also catalyzes the conversion of the DA in excess to neuromelanin, an insoluble dark pigment that can be found in aged DA neurons [29, 48].

Generally the brain regions responsible for motor functions seem to have more iron than non-motor related regions explaining why movement disorders are often associated with iron concentration [29].

So, iron is a very important element in the brain but in excess it is responsible for the production of ROS and consequent neural damage. Therefore, the cell must guarantee that this element is in equilibrium [25].

Copper is a redox active transition metal occurring in two main oxidation states, +2 and +1. As such, it is also associated with the generation of ROS because it participates in Fenton reactions in a process similar to iron [29].

Besides this mechanism, copper modulates oxidative stress by also reducing the levels of glutathione. Normally glutathione (GSH) concentration in the cells is in the millimolar range. GSH acts as potent cellular antioxidant and as substrate for several enzymes removing ROS. Glutathione is involved in intracellular copper metabolism and it can modulate copper toxicity by directly coordinating the metal with high affinity. Moreover the stabilization of copper reduced state, makes it unavailable for redox cycling [29].

Also contributing to the defense against oxidative stress is cytosolic copper-zinc superoxide dismutase (CuZnSOD), which convert superoxide to O_2 and H_2O_2, are important as enzymatic defenses. Decreases in CuZnSOD activity can lead to a perturbation of cellular antioxidant defense mechanisms and promote oxidative stress.

In addition of copper involvement in the oxidant environment of the cells, this ion also binds with α-syn. This interaction results in the generation of unique toxic forms of oligomers, which are α-Syn varieties capable of inducing formation of pores in the cellular membrane, changing the intracellular ionic balance, triggering apoptosis, affecting functions of mitochondria, intensifying degradation of proteins and inducing oxidative stress [49].

Zinc (Zn) is the most abundant trace metal in the brain where it plays various functions. It interacts with several proteins conferring on them catalytic or structural properties. Zinc is released into the synaptic cleft and it modulates some receptors regulating the activity of glutamatergic synapses, suggesting its possible role as a neurotransmitter on its own. Several different factors, such as balance between the cellular redox state, the concentrations of other biological chelating agents and the energy status of the cell are determinant for zinc distribution within the cell [29].

Contrary to copper and iron, zinc is a redox inert metal and does not take part in oxidation-reduction reactions. However zinc deficiency has been associated with increased levels of oxidative damage including increased lipid, protein and DNA oxidation. Zinc can act as an antioxidant [8] by protecting sulfhydryl groups of proteins against free radical attack. Such as iron and copper and has a key role in the immune system, through its prevention of membrane peroxidation by Cu/Zn superoxide dismutase (Cu/Zn SOD) [5, 30].

1.4. Parkinson's disease Models

There are several experimental models of PD. They can be divided into two main groups, the toxin based models and the genetic mutations models. The toxin based models, in which is included the model used in the present work, can reproduce the pathologic hallmarks of PD, still there are some deviations from the disease. For example, using these kind of models the degeneration of dopaminergic neurons occurs quickly, days, instead of years as happens in the real state of the disease [38].

MPTP (1-methyl-4-phenyl-1,2,3,6-tetrahydropyridine) has been a toxin of choice for investigations into the mechanisms involved in the death of dopaminergic neurons in PD [50]. MPTP primarily causes damage to the nigrostriatal DA pathway with a profound loss of DA in the striatum and SNpc. This specific and reproducible neurotoxic effect on the nigrostriatal system is the strength of this model [38].

Like MPTP, 6-hydroxidopamine (6-OHDA) is a selective catecholaminergic neurotoxin that is used, mainly, to generate lesions in the nigrostriatal DA neurons in rats. Since 6-OHDA cannot cross the blood-brain barrier, systemic administration fails to induce PD. So, to overcome this issue, 6-OHDA is directly injected (typically as a unilateral injection) into the SNpc, medial forebrain bundle or striatum. The effects resemble those in the acute MPTP model, causing neuronal death over a brief time course (12 h to 2–3 days). The intrastriatal injection of 6-OHDA, causes progressive retrograde neuronal degeneration in the SNpc. As in PD, DA neurons are killed, and the non-DA neurons are preserved [38].

Chronic systemic exposure to rotenone in rats causes many features of PD, including nigrostriatal dopaminergic degeneration [51]. The rotenone administered animal model also reproduces all of the behavioral features reminiscent of human PD. Importantly, many of the degenerating neurons have intracellular inclusions that resemble LB morphologically. Usually, rotenone is administered by daily intra peritoneal injection, intravenously or subcutaneously [52].

Paraquat (1, 1-dimethyl-4,4'-bipyridinium dichloride), the toxin used in this work, is a quaternary nitrogen herbicide widely used for broadleaf weed control. It is a fast-acting, non-selective compound which destroys tissues of green plants. Various pesticides and herbicides are intensively used annually worldwide, with rotenone and paraquat (PQ) being only two of the many agricultural chemicals known to affect the dopamine systems. [53].

For many years, concerns about PQ exposure were focused on its effects on lung, liver and kidney because acute exposure to this pesticide in these organs can result in death. Then it was observed that PQ was structurally similar to MPTP and the hypothesis of neurotoxicity

was considered. Furthermore, there are studies that suggest an increased risk for PD due to PQ use [53].

There are studies showing that a repeatedly administration of PQ for 5 days to 6 weeks in rats produces a decrease in the number of dopaminergic neurons of the SN. The toxicity of this herbicide to this specific kind of neurons may be due to the fact that it specifically accumulates in neuromelanin containing neurons [54].

The cellular toxicity of PQ is essentially due to its redox cycle including a well-known cascade of reactions leading to NADPH consumption and to generation of ROS mainly hydrogen peroxide (H_2O_2) and hydroxyl radical ($HO^{\cdot}$) with consequent cellular toxic effects [55]. Indeed, lipid peroxidation has been suggested as a potential mechanism of toxicity during exposure to PQ *in vitro* and *in vivo* [56].

PQ exposure also induces movement disorders in some mammalian models and it's responsible for an increased level of α-Syn which is followed by α-Syn aggregation in the SNpc neurons[55, 57].

Because of the toxicity upon dopaminergic neurons, PQ is responsible for a decrease of dopamine concentration in striatum terminal, which induces neurobehavioral syndrome characterized by locomotion reduction [53, 55].

Table 1.3 shows a summary of the models that were listed above and its consequences in terms of loss of neurons in the SNpc, the loss of dopamine in striatum and the aggregation of α-Syn (Lewy bodies).

Table 1.3. - Toxin based animal models for Parkinson's disease and its characteristics. Table adapted from Blesa, J. and Przedborski, S., 2014 [38].

Animal Model	Motor Behavior	SNpc neuron loss	Striatal loss	Lewy Body/α-Syn pathology
MPTP	Reduced locomotion, Bradykinesia	↑ ↑ ↑	↑ ↑ ↑	No
6-OHDA	Reduced locomotion, Altered behavior	↑ ↑ ↑	↑ ↑ ↑	No
Rotenone	Reduced locomotion	↑ ↑	↑ ↑ ↑	Yes
Paraquat	Reduced locomotion	↑ ↑	↑ ↑ ↑	Yes

Besides the toxin based animal models there are others, based on genetic mutations, that are also able of reproduce the pathological characteristics of PD. In this work only the toxin based ones are referred because, as it has been mentioned above, a PQ model was used in our experiments.

1.5. Objectives

The main objectives of this work are the optimization of the operational parameters of a commercial, non-dedicated, X-ray fluorescence spectrometer so we can be able to identify several atomic elements in two specific regions of the brain of a PD rodent model and to see if we can establish differences in the concentrations of the atomic elements between two groups, a control and a Paraquat treated group.

Chapter 2 – Experimental Setup, Material and Methods

2.1. Experimental Setup

2.1.1. General Description

The measurement of brain tissue atomic elements were performed with the X-ray fluorescence spectrometer, model SEA6000VX from Hitachi High-Tech Science Corporation, figure 2.1, which performs qualitative and quantitative analysis of elements present in samples. This instrument was designed to perform multi-element spectroscopy and spectrometry.

Figure 2.1 – Photography of SEA6000VX X-ray fluorescence spectrometer [58].

There are several steps in generating fluorescence X-rays from a sample. SEA6000VX use the simplest type of X-ray tube to generate fluorescence X-rays. Primary X-rays produced by an X-ray tube irradiate the sample. After the X-rays are produced, they pass through the collimator so the size of the beam in the sample is set. Next, the beam passes through a filter that selects the energy range that will excite the elements in the sample [17].

After leaving the sample the emitted characteristic fluorescence X-rays are detected by a semiconductor detector being its energy measured. The multichannel analyzer (MCA) makes the distribution of the X-rays detected (counts) per small energy intervals (designed by energy bin or channel) resulting in an energy spectrum. The counts accumulated in each channel correspond to the X-rays intensity at that energy. The atomic elements in a substance can then be found by semi-qualitative analysis [17].

The image of the sample is obtained by a CCD camera and displayed on a computer screen making accurate positioning easy. Beyond the image a guiding grid is also represented in the screen, the center of that grid corresponds to the measurement position center [17]. An image of this screen is depicted below in figure 2.4.

A controller joystick and a Z-axis control button allow the user to freely move the sample platform in any of the three axes directions (X, Y and Z). Adding this to the fact, mentioned above, that the position can be checked on the monitor makes the positioning of the measurement point more easy and fast [17].

2.1.2. X-ray tube

The X-ray tube is a vacuum tube that produces primary X-rays. The X-ray tube contains a filament that when an electric current crosses it, heats up the cathode electrode leading to thermionic emission of electrons. Then the electrons are accelerated by a high voltage and collide with a metal anode (target), producing primary X-rays. The X-ray tube is illustrated in the figure 2.2 below.

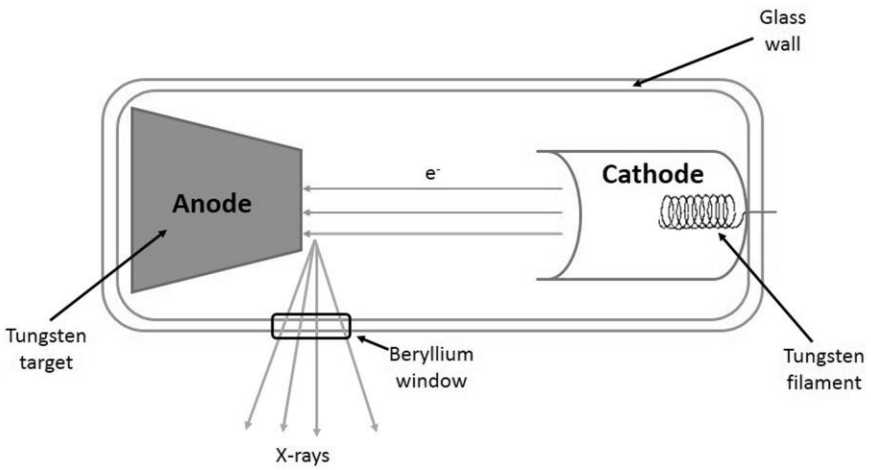

Figure 2.2 – Scheme of an X-Ray tube. Image adapted from SEA6000VX Operation Manual, Hitachi High-Tech Science Corporation, 2013 [17]. The maximum current selectable was 1000 μA and the voltage 50 kV.

As electrons strike a target, most of the kinetic energy of the electrons is converted into heat. Only about 1% (or less) of the kinetic energy is converted into X-rays. The anode can be made of several kinds of materials, in the case of SEA6000VX, it's a tungsten anode. Besides producing characteristic X-rays from atoms characteristic of the anode element, an X-ray tube also generates continuous X-rays from *Bremsstrahlung* X-rays, as referred above in section 1.1.2. The voltage applied determines the energy of the electrons that hit the anode and therefore the maximum energy of the X-rays that leave the tube.

2.1.3. X-ray collimator

The generated X-ray beam propagates in a wide beam. The X-ray beam applied to a sample must be very narrow, being the size controlled by the user. The collimator constricts the dimensions of the X-ray beam on the sample. It is formed by an open metallic cylinder where the incident X-rays cannot penetrate its walls. A collimator is represented in figure 2.3 below.

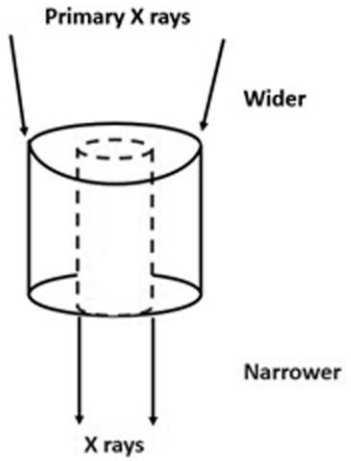

Figure 2.3 – Scheme of the collimator. Image adapted from SEA6000VX Operation Manual, Hitachi High-Tech Science Corporation, 2013 [17].

2.1.4. X-ray filters

The X-ray fluorescence spectrometer allows to choose between five X-ray filters (Cl, Cr, Pb, PbMap and UNI) and no filter at all. The filters allow the tuning the incident X-rays energy band with the excitation energy of the atomic elements. This is implemented via the partial photoelectric absorption of the incident X-rays by the selected filter's material. Hereupon, and taking in to account the atomic elements that we want to measure, the filters that we choose to work (see section 3.1 below) were Cl (to measure low Z elements: P, S, Cl, K and Ca), Cr (to measure the low Z elements and Fe) and PbMap (to measure the transition metals: Fe, Cu and Zn).

2.1.5. X-ray detector

The X-ray fluorescence spectrometer is based on a multi-cathode Si semiconductor detector, which is characterized by an excellent energy resolution in the low energy band, 1–10 keV, having the ability to measure, during the same period of acquisition, the X-rays energies emitted from the low-Z elements of the sample. The detector has a beryllium window, which has low-Z and thus having high transparency to the incident X-rays on the detector.

Traditional X-ray fluorescence spectrometers require cooling of the detection system (detector and front-end electronics) by liquid nitrogen (~-196 ºC) in way to achieve the desired energy resolution. This spectrometer has a liquid nitrogen-free detector, where the necessary moderate cooling (~-30 – -40 ºC) is implemented by a thermoelectric cooler (Peltier cell).

Approach of the sample to detector is a key factor to achieve worthy measurements. However, to prevent sample collision with X-ray detector, the system has an auto-set of sample height and a collision prevention system.

2.1.6. CCD Camera

This system has a CCD camera that shows on the PC-monitor the image of the sample on the sample-holder. This is very useful to the user because this way positioning the sample becomes an easier task. Besides, the center of image corresponds to the center of the X-ray beam and the size of it in the sample is also shown. In figure 2.4 is depicted the image of the sample for one of our measurements, using a 3.0×3.0 mm^2 X-ray beam in which all of these characteristics can be seen.

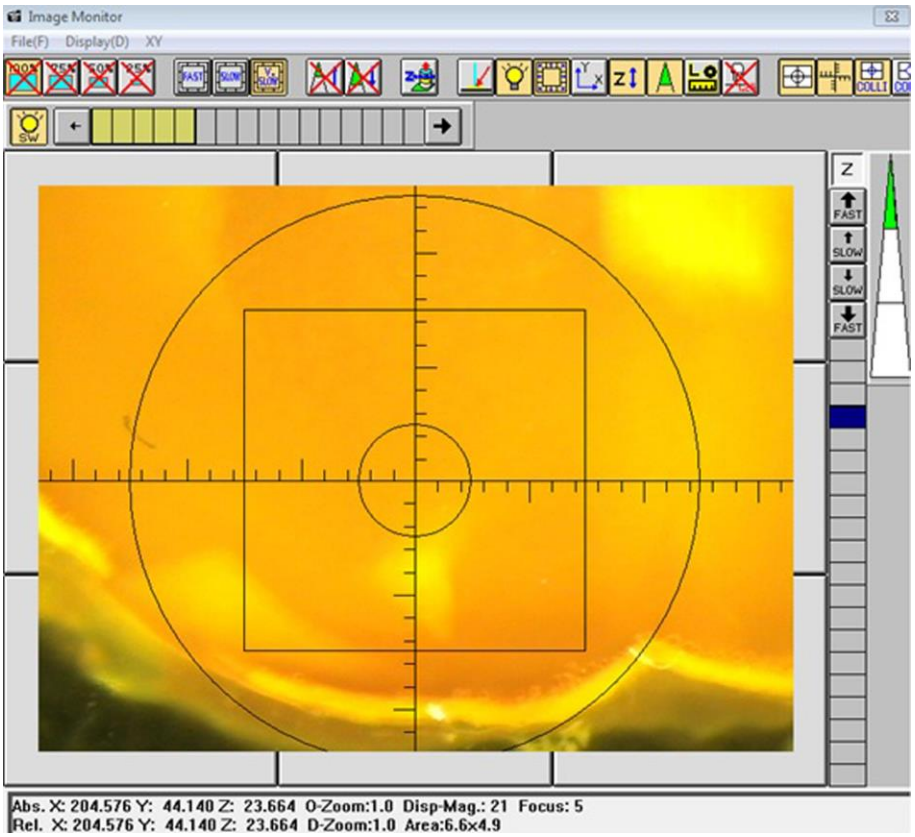

Figure 2.4 – Image provided by the CCD camera and all the commands available. The square on the picture represents the X-ray beam.

2.1.7. Gas System

This system has the option of using a helium flow to eliminate argon of air. As we attempt to measure some low-Z elements, and argon could interfere with some of them, we use the helium at a rate of 2L/min that is the value recommended.

2.1.8. Software

All the features of SEA6000VX X-ray spectrometer are controlled by the associated software, X-ray Station. This software facilitates the control of the equipment and makes the process of measurement simpler. The system software also allows the user to select measurement conditions, like the time of measurement, voltage, electric current, size of the beam, filter type, gaseous environment (air or He purge) and peaking-time of the front-end electronics. A typical window of the measurement conditions is represented in figure 2.5.

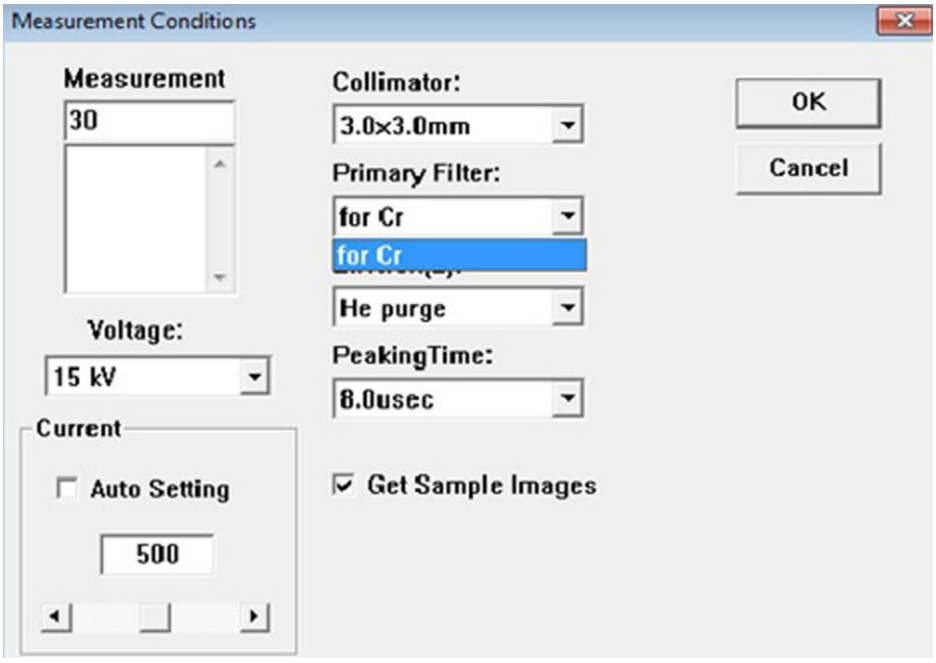

Figure 2.5 – Measurement conditions selection window.

The layout of the software is depicted in figure 2.6. The first image (figure 2.6 a) represents the screen in which we can see, in the upper left side, the whole X-ray energy spectrum from 0 to 40 keV. Below the energy spectrum are represented the elements selected to analyze, the X-rays intensity in counts per second and the region-of-interest (ROI) selected by the software. The central image shows the region of the energy spectrum selected by the user and, on the right side, the selected conditions of measurement are represented.

Beyond parameter selection, the software also allows the user to choose the elements in a periodic table to analyze (figure 2.6b, left side). The peaks of these elements will be highlighted in the energy spectrum as it's shown in figure 2.6 a. The CCD camera image that we have already mentioned is also displayed on this screen.

a)

b)

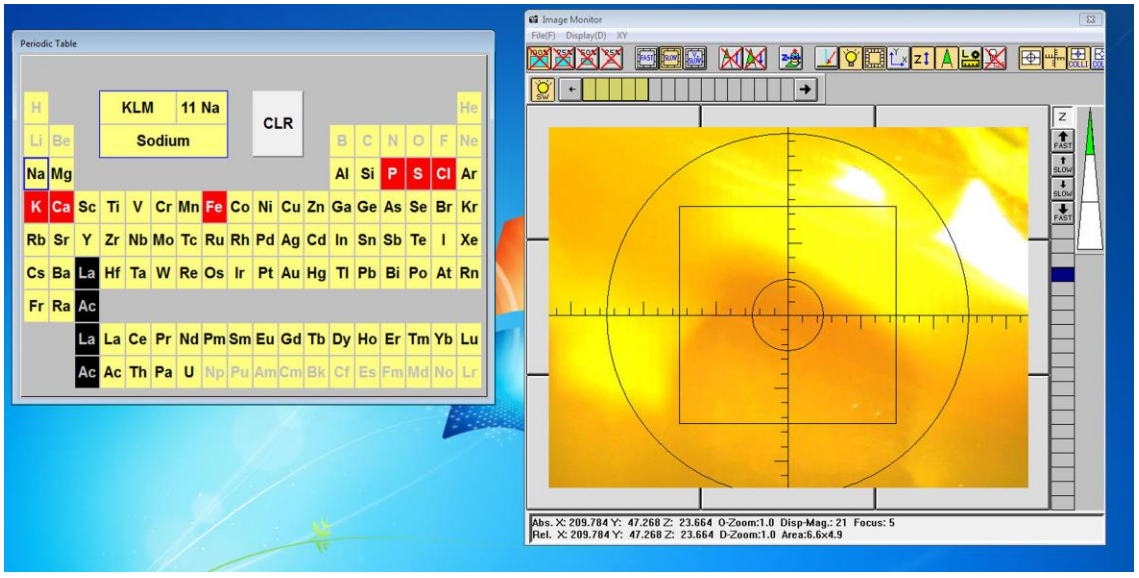

Figure 2.6 – Visual layout of the software (see text). Each image is displayed in an individual monitor (two monitors).

2.2. Materials

2.2.1. Tissue Samples

Tissue samples were prepared at CICS facilities, University of Beira Interior. The experiments were performed on rats, in compliance with protocols approved by the national ethical requirements for animal research, the European Convention for the Protection of Vertebrate Animals Used for Experimental and Other Scientific Purposes (European Union Directive number 2010/63/EU). All procedures were approved by the local Animal Care and Use Committee. Male Wistar rats (8–10 weeks) were maintained in a temperature/humidity-controlled environment under a 12 light/dark cycle with *ad libitum* access to food and water.

Each animal received four intraperitoneal injections, separated by 1 day, of either vehicle (saline) or paraquat (PQ) (10 mg/kg body weight), according to a previously published dose. Five days after the last PQ intraperitoneal injection, animals were killed [59].

Samples were cut on a coronal brain matrice that allows cuts of 1mm slices minimum. To include the total region of interest (*substantia nigra*, SN and *striatum*, ST), each slice were cut with 3 mm of thickness. This value was also chosen based in the optimization done with the X-ray fluorescence spectrometer. This optimization is described next in section 3.1.

These experiments used 9 rats, 5 treated with PQ and 4 control. For each rat there were two cerebral slices, one of SN and one of ST.

2.2.2. Tissue Frames

Tissue frames, represented in figure 2.7, were also prepared on CISC facilities, University of Beira Interior. This assembly used plastic square frames with $\approx 3.0 \times 3.0$ cm^2 open area and ≈1.7 mm thickness. First, a 7.5 μm Kapton foil was glued to one side of the frame. Next the tissue slice was deposited on this foil and a second Kapton foil with the same thickness was glued to the frame to cover the tissue. The Kapton foil was used due to its high transparency to low energy X-rays.

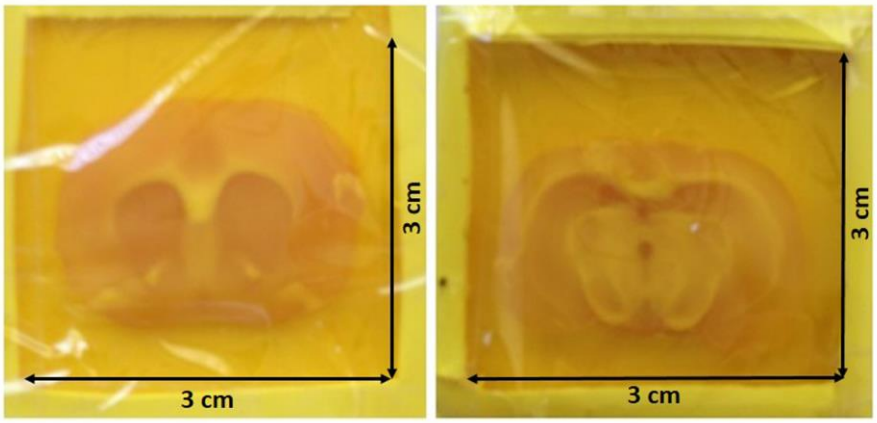

Figure 2.7 – Photographs of two assembled frames with tissue slices: (left) a slice of ST and (right) a slice of SN.

To do the measurements, these tissue frames were placed upon a ≈ 2 cm thickness Perspex base, being approximately ≈ 3 mm away from the detector window. The Perspex base was placed over the system translational (XYZ) platform.

2.3. Fluorescence intensity measurement methods

2.3.1. Selection of the irradiation sample's region

The selection of the irradiation sample's region was made taking in to account the information of the Atlas with the rat brain in stereotaxic coordinates [60]. Is should be stressed that the dimensions depicted in the Atlas are typical dimensions, not necessarily equal to the dimensions in our tissues.

2.3.1.1. In *substantia nigra*

In the case of *substantia nigra*, the cut was made from bregma coordinate -2.3 mm, anterior side (see figure 2.8 a) to -5.6 mm, posterior side (see figure 2.8 b). The irradiation was made on the posterior side.

a)

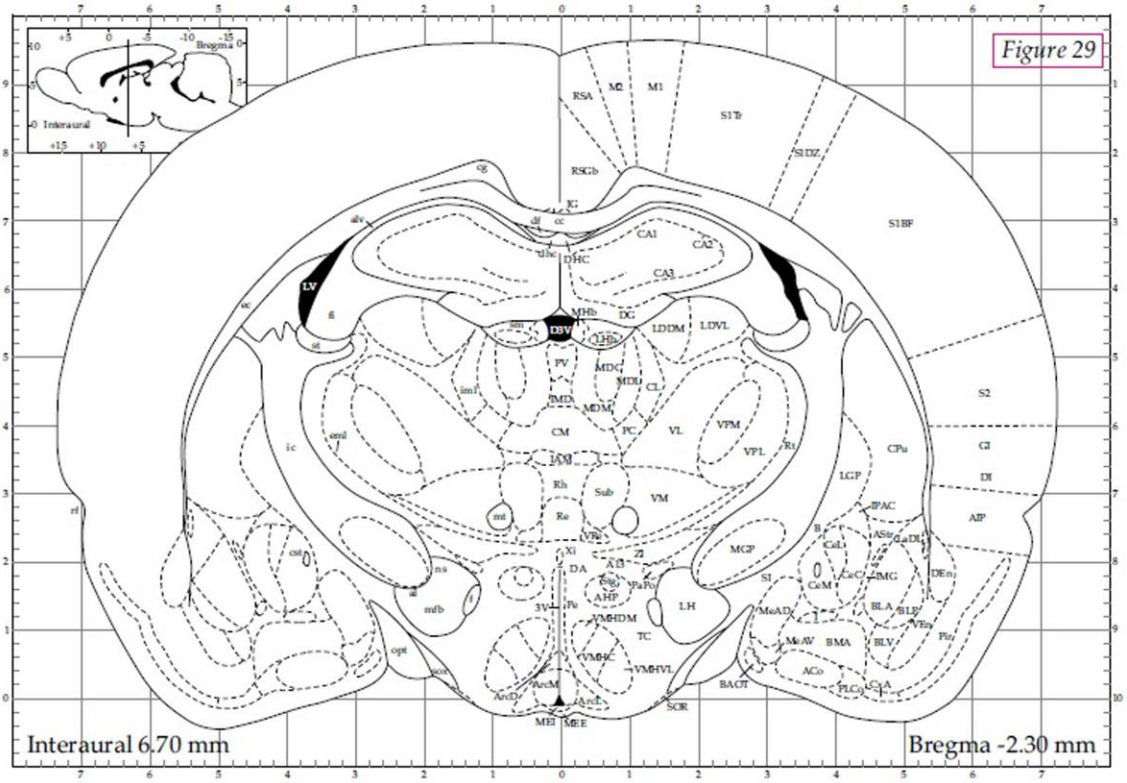

b)

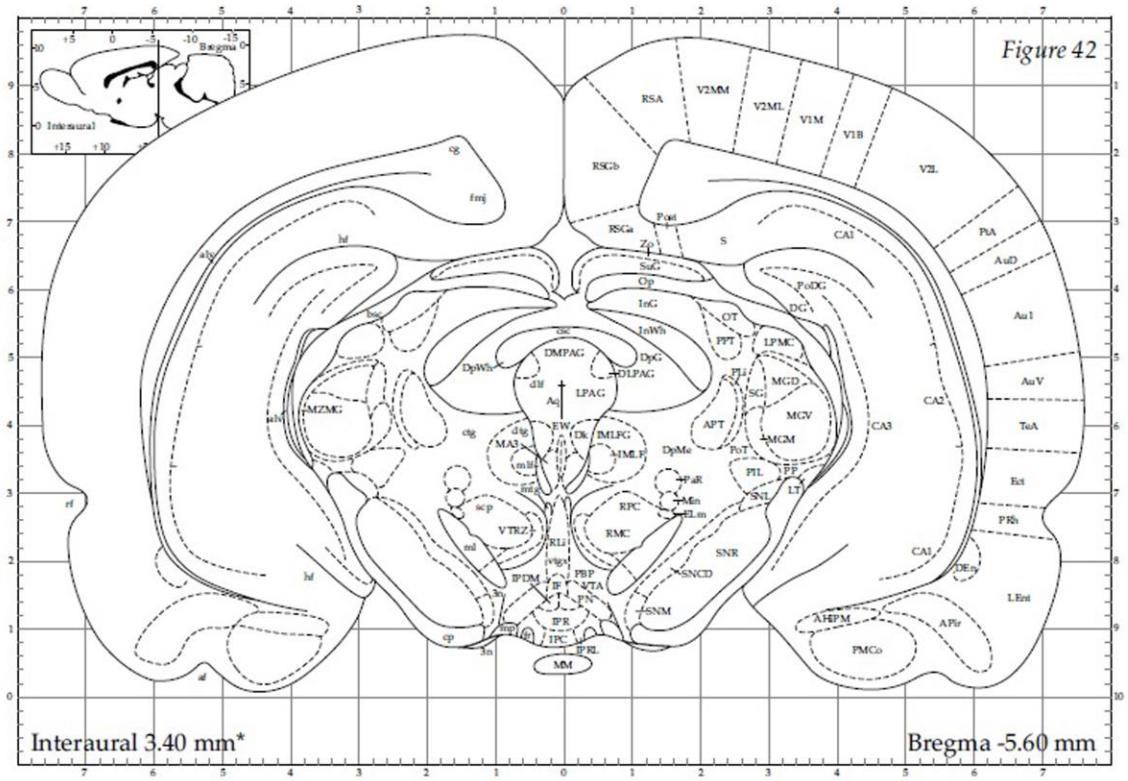

Figure 2.8 – Atlas images of SN borders, the first image a) represents anterior side and b) the posterior [60].

2.3.1.2. In *striatum*

In the case of *striatum*, the cut was made from bregma coordinate 1.7 mm, anterior side (see figure 2.9 a)) to -1.3 mm, posterior side (see figure 2.9 b)). The irradiation was made on the anterior side.

a)

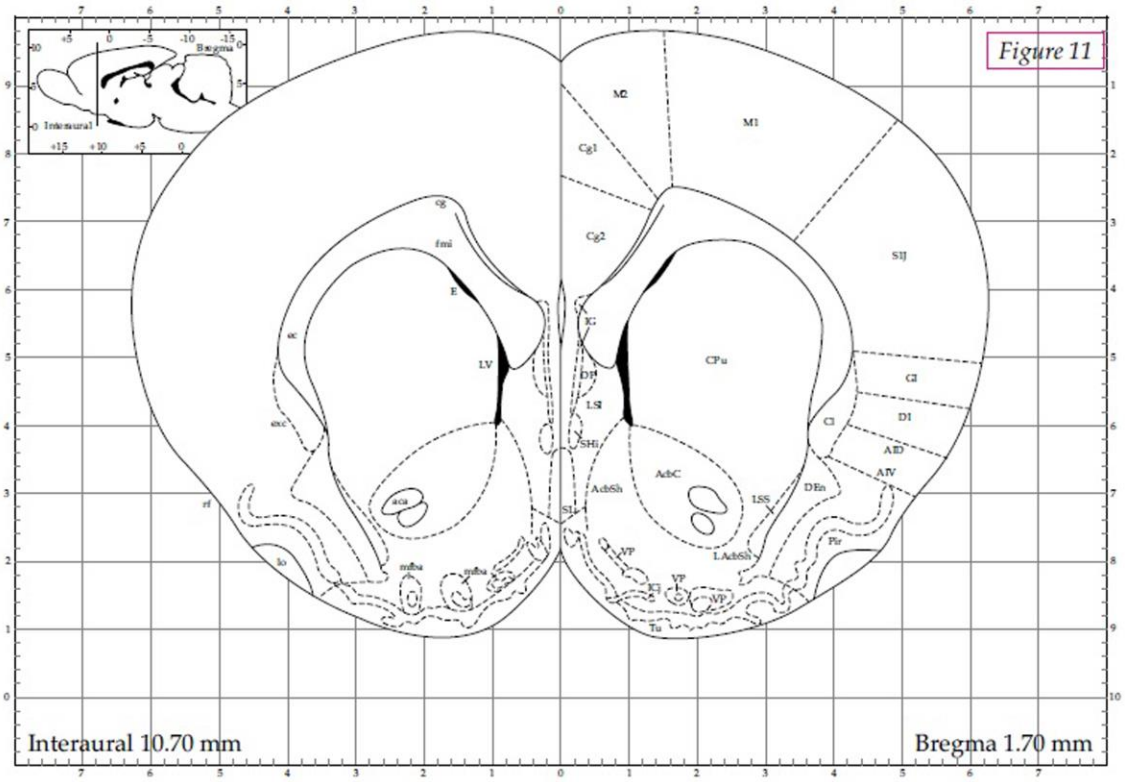

b)

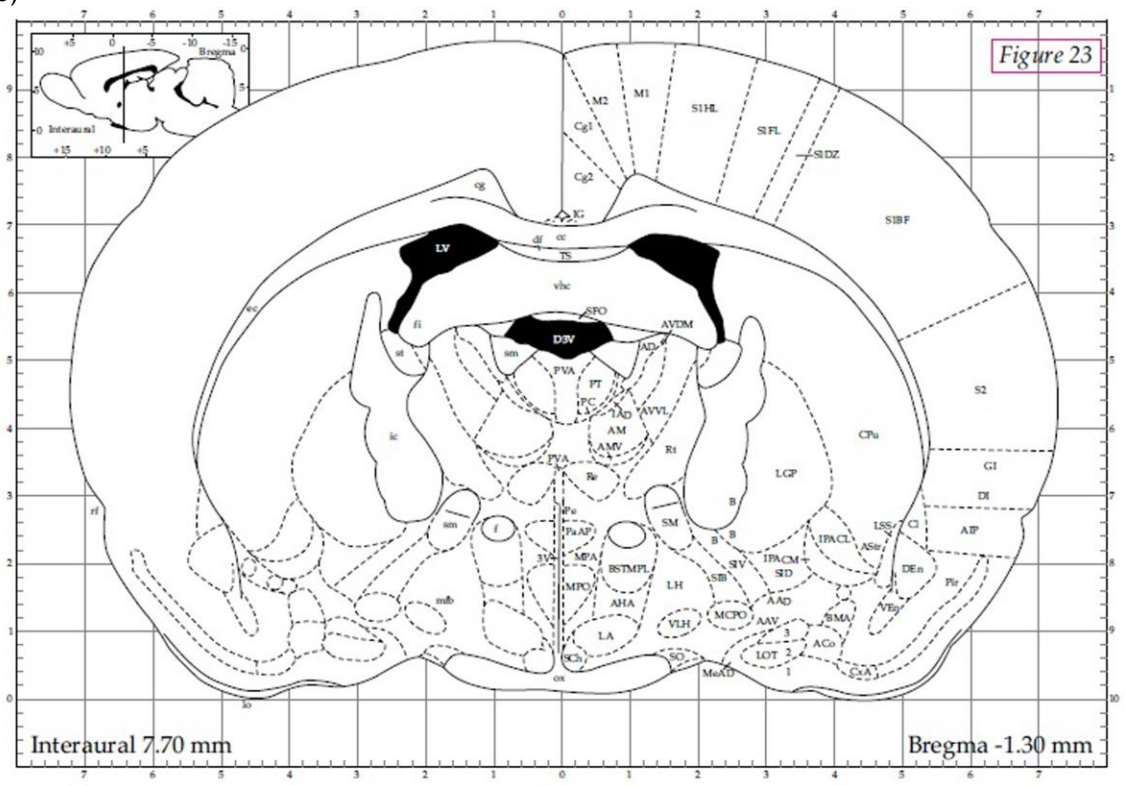

Figure 2.9 – Atlas images of ST borders, the first image a) represents anterior side and b) the posterior [60].

2.3.2. Selection of the dimensions of the sample

The selection of the dimensions of the X-ray beam on the sample was made based on Atlas images [60] shown previously and in the measurement of the tissue samples using the system of coordinates(XY) supplied by the spectrometer. This helped us to decide the size of the beam that we should use to cover the maximum possible area of each structure. The figure 2.10 depicts a tissue sample with the SN regions. The blue lines delimit the SN areas and the grey squares the 1.2×1.2 mm^2 beams used to irradiate this zone.

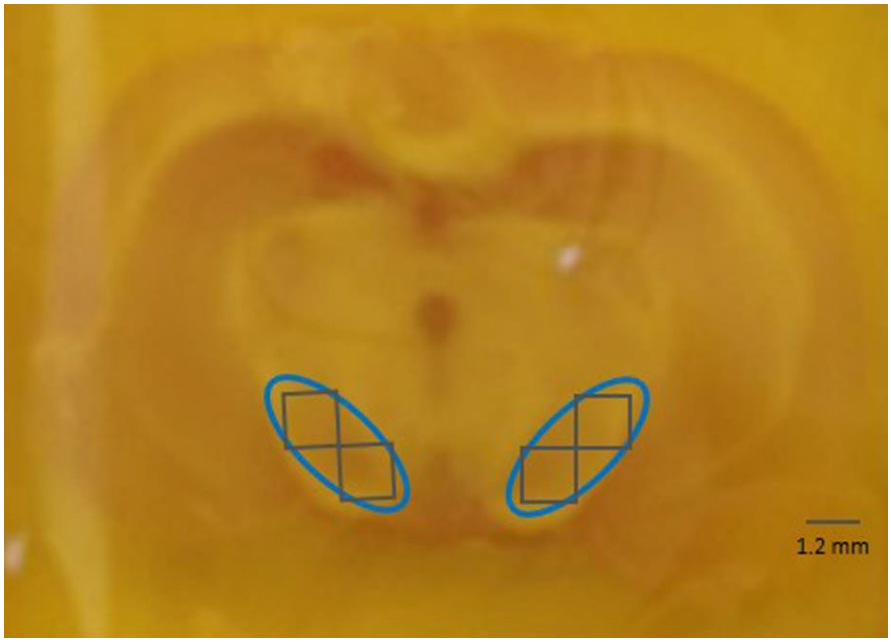

Figure 2.10 – Example of a tissue sample used in SN measurements. The blue circles represent SN and the grey squares the beams with which it was irradiated.

For the case of ST regions, we choose to irradiate the sample two times with a 3.0×3.0 mm^2 beams, as it's represented in figure 2.11 below.

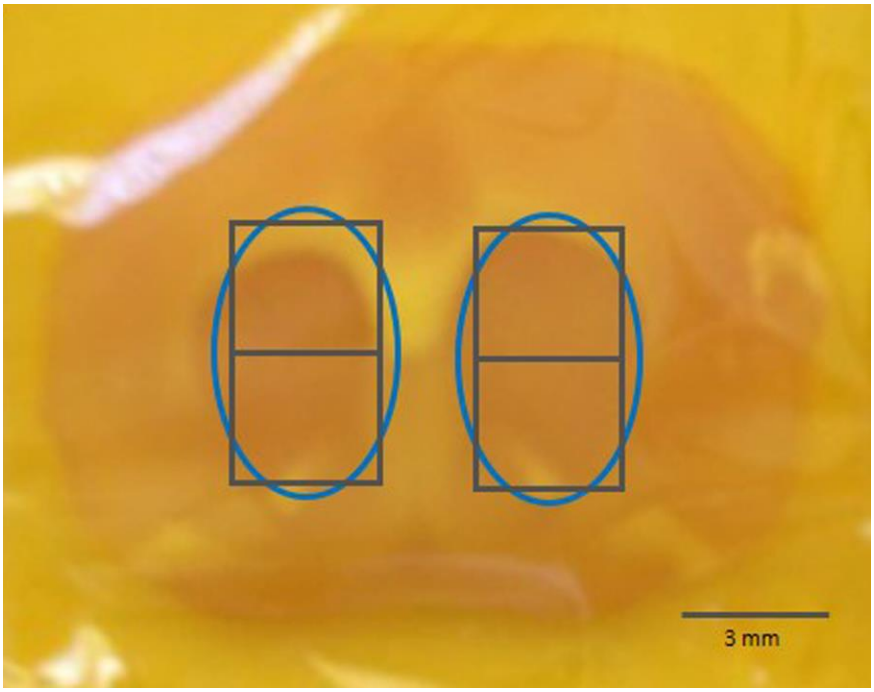

Figure 2.11 – Example of a sample used to ST measurements. The blue circles represent the ST and the grey squares the beams with which it was irradiated.

2.3.3. Calculation of the elements peak area/ X-ray fluorescence intensity

2.3.3.1. Region of interest (ROI)

Region of interest (ROI) is an interval of energy in which the system considers are the counts of a given element. The ROI is characteristic of the elements and change with the ability of the system to discriminate the energies, i.e. with the energy resolution, being larger in the case of ST measurements, because the lower peaking time of 1 μs used in front-end electronics, resulting in higher electronic noise and thus in worst energy resolution.

Table 2.1 – Values of ROI (K_α X-rays) for 8 μs of peaking-time.

Z	Elem Name	Kα Energy (keV)	ROI (keV)
15	Phosphorus (P)	2.014	1.90 - 2.13
16	Sulphur (S)	2.308	2.19 - 2.42
17	Chlorine (Cl)	2.622	2.50 - 2.74
19	Potassium (K)	3.313	3.19 - 3.44
20	Calcium (Ca)	3.691	3.56 - 3.82
26	Iron (Fe)	6.400	6.25 - 6.55
29	Copper (Cu)	8.042	7.87 - 8.21
30	Zinc (Zn)	8.631	8.46 - 8.80

Table 2.2 – Values of ROI (K_α X-rays) for 1 μs of peaking time.

Z	Elem Name	Kα Energy (keV)	ROI (keV)
15	Phosphorus (P)	2.014	1.88 - 2.15
16	Sulphur (S)	2.308	2.17 - 2.45
17	Chlorine (Cl)	2.622	2.48 - 2.77
19	Potassium (K)	3.313	3.16 - 3.46
20	Calcium (Ca)	3.691	3.54 - 3.84
26	Iron (Fe)	6.400	6.23 - 6.57
29	Copper (Cu)	8.042	7.86 - 8.23
30	Zinc (Zn)	8.631	8.44 - 8.82

2.3.3.2. Gaussian and linear fittings

After the acquisition we had the raw data from SEA6000VX spectrometer, but that data (X-ray counts) for each atomic element detected included background counts that must be excluded in way to obtain the element X-ray fluorescence intensity, i.e. the X-ray fluorescence counts. Several methods could be implemented to perform this task.

Initially the method to subtract the background counts consisted in define a horizontal straight line below the respective element peak in the energy spectrum, then the straight line parameter was measured and multiplied by the number of energy bins (channels) in the element ROI, and then the resulting value was subtracted to the total number of counts in the ROI given by spectrometer. The problem with this method is that it could be subjective. Hereupon and as the atomic elements are depicted in the X-ray energy spectra in the form of Gaussian peaks, it was decided to perform Gaussian fittings to the peaks with the software OriginPro8. From the fittings it was extracted the parameters of the Gaussian function: the centroid (element energy), standard deviation (width) and area (which measures the element X-ray fluorescence counts), and the parameter for the baseline (which measures the background counts).

The Gaussian fitting was performed by selecting the ROI (for the K_α X-rays) of each atomic element, then the software OriginPro8 provided a table with all the Gaussian parameters and baseline parameter.

The fittings are shown in figure 2.13 below. This method was applied to obtain phosphorus, sulfur, chlorine and potassium X-ray fluorescence counts with filters to chloride (Figure 2.13a) and to chromium (Figure 2.13b) and iron, copper and zinc X-ray fluorescence counts with filter to PbMap (Figure 2.13c).

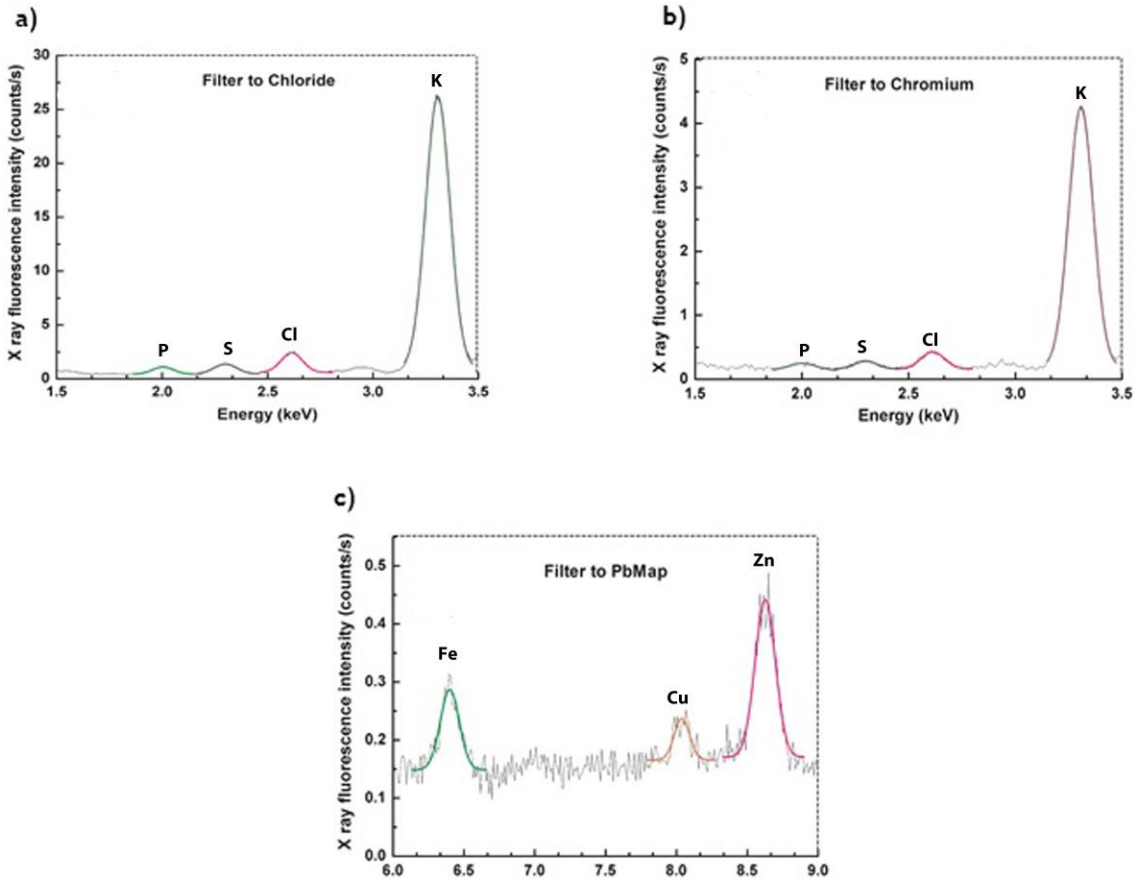

Figure 2.12 – Gaussian fittings: a) spectrum using filter to chloride with peaks of phosphorus, sulfur, chloride and potassium; b) spectrum using filter to chromium with peaks of phosphorus, sulfur, chloride and potassium; c) spectrum using filter to PbMap with peaks of iron, copper and zinc.

In the case of Fe peak with filter to Cr, a regular Gaussian fitting won't be enough because the peak was set upon a sloping line. In this case we create a function using Fitting Function Organizer tool, also from the software OriginPro8 that consisted in a sum of a linear and a Gaussian function. Both, graph and fitting function (see figure 2.13 below).

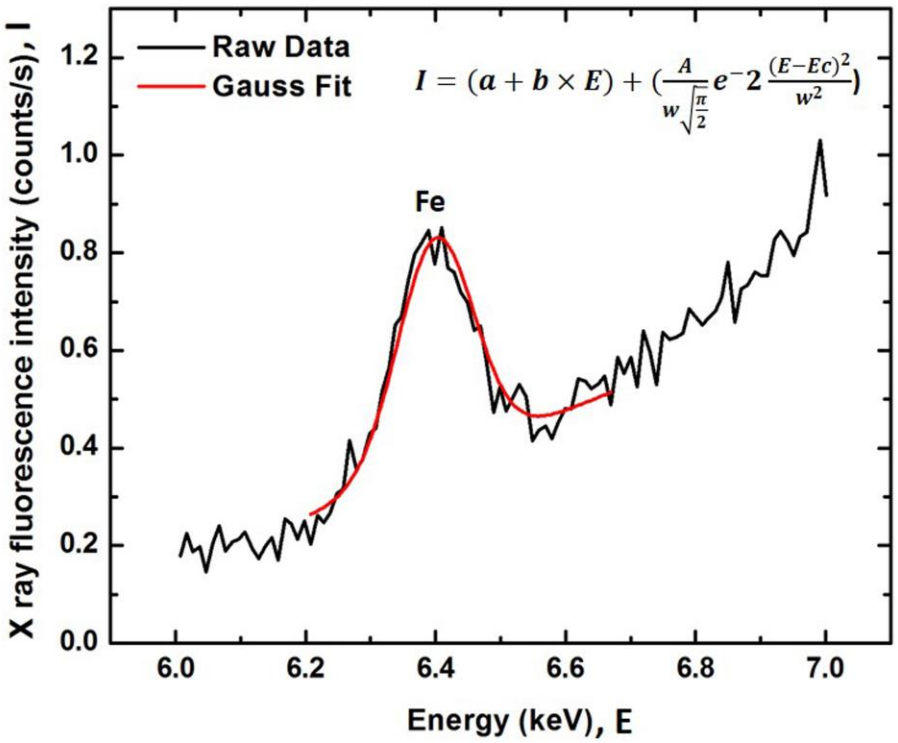

Figure 2.13 – Iron peak and it's fitting (represent in red) with the sum of a linear function with and a Gaussian function. The fitting function is also represented.

2.3.1.3. The energy resolution method for Ca metal

Since the first measurements became clear that the spectrometer wouldn't able to distinguish between the K K_β X-rays (energy 5.59 keV) peak and the Ca K_α X-rays (energy 5.69 keV) peak. Thus the overlap of these peaks of neighboring elements (K and Ca) does not enable the determination of the area parameter of the Ca peak via the regular Gaussian fittings (see above) and consequently the Ca X-ray fluorescence intensity. To overcome this problem we decide to create another function in OriginPro8 that consisted in the sum of two Gaussian functions, one to fit the K peak and the other to fit the Ca peak.

To implement this fitting correctly in way to extract the true area of the two peaks it was fixed all the two Gaussian functions parameters but the areas. The correct energy calibration of the spectrometer allows using the respective X-rays energy from the literature as centroid parameters values and the corresponding width parameters values were determined in an extra-experiment implemented to measure the energy resolution of the spectrometer versus

the energy of fluorescence X-rays, i.e. the *Full Width at Half Maximum,* FWHM (or the width, *w*) for several X-ray energies within 1.5–6.5 keV range.

To obtain the *w* values for the K K_β and Ca K_α X-rays peaks we irradiated in the spectrometer several pure samples of silicon, sulfur, chloride, calcium, titanium, chromium, manganese and iron, and measured via Gaussian fittings the respective *w* (FWHM) values versus the K_α X-rays energy of each element. Two runs were performed, one with conditions for SN measurements (1.2×1.2 mm^2 X-ray beam and 8 μs peaking-time) and other with conditions for ST measurements (3.0×3.0 mm^2 X-ray beam and 1 μs peaking-time).

The measured FWHM values versus X-rays energy are depicted in figure 2.15. A fit to the FWHM data was implemented, using a function with two parameters represented below in table 2.4.

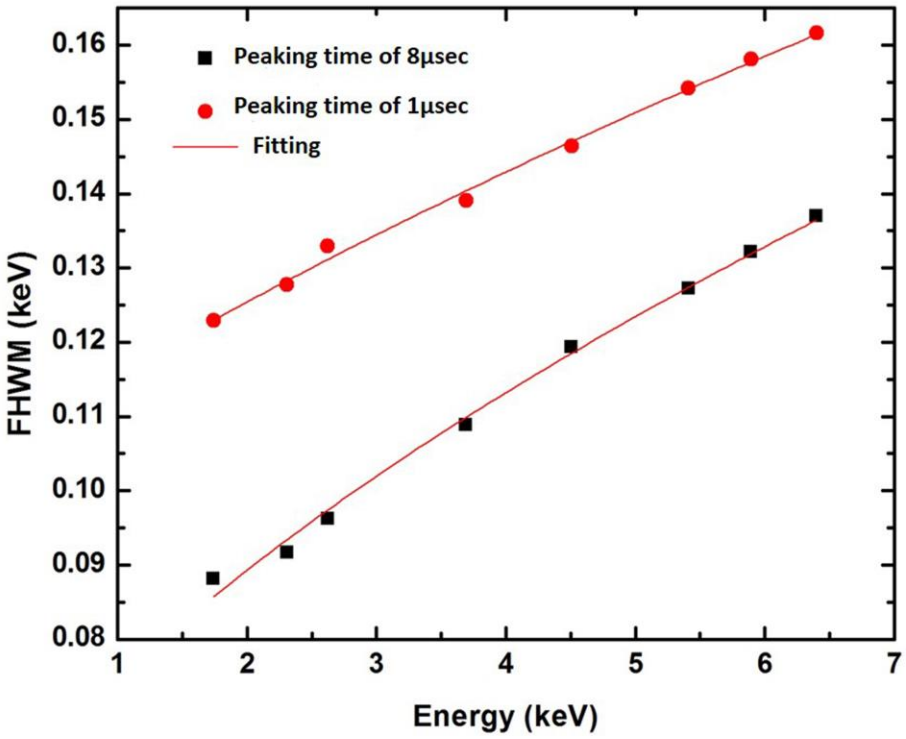

Figure 2.14 – FWHM vs K_α energy for 1.2×1.2 mm^2 beam (black squares) and 3.0×3.0 mm^2 beam (red circles). The fitting is represented in both cases by a red line. The fitting function is also showed.

Table 2.3 – Parameter values obtained from the fit to FWHM data.

$FWHM = \sqrt{a + b * E}$	**Peaking time of 8μs**	**Peaking time of 1μs**
a	$(31.4 \pm 2.7) \times 10^{-4}$	$(110.4 \pm 2.5) \times 10^{-4}$
b	$(24.2 \pm 6.9) \times 10^{-5}$	$(23.5 \pm 6.2) \times 10^{-5}$

Thus, from the FWHM fit function, it was obtained the FWHM (and *w*) values for the K K_β energy (3.59 keV) and for the Ca K_α energy (3.69 keV), being the values of *w* equal to 0.0926 and 0.0935 keV, respectively, with conditions for SN measurements. With conditions for ST measurements, the values of *w* obtained were equal to 0.11877 and 0.11949 keV, respectively.

Lastly, the double Gaussian fit could be implemented, with the two area and baseline parameters free (see figure 2.15 below).

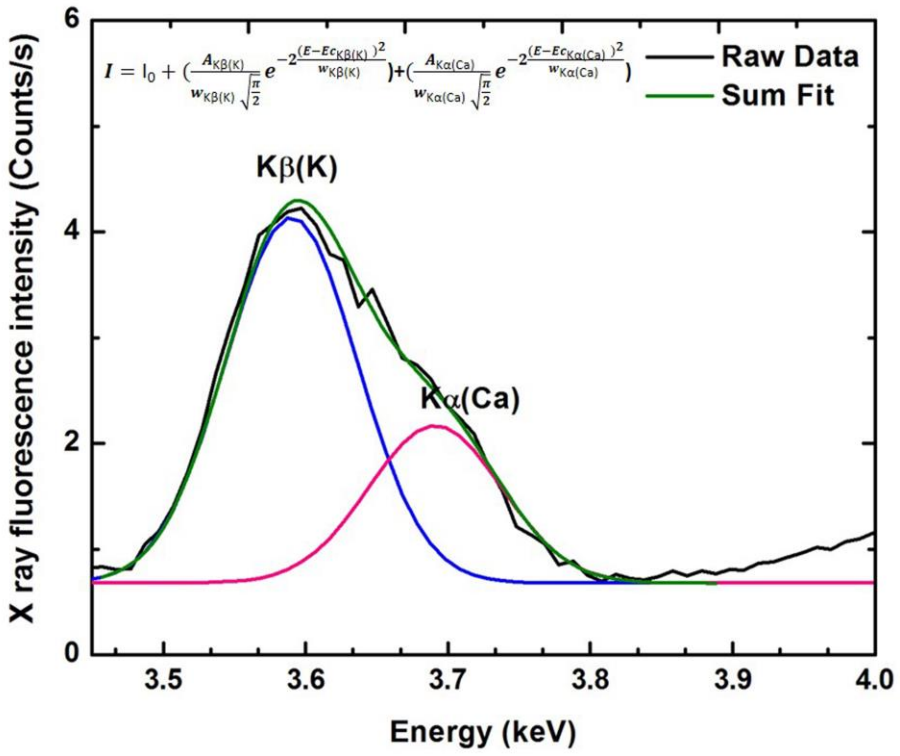

Figure 2.15 – Example of double Gaussian fit to obtain Ca X-ray fluorescence intensity. In black it's represented the original sum peak (resulting from K K_β (energy 5.59 keV) and the Ca K_α X-rays (energy 5.69 keV)), green is the double Gaussian fit, blue line is K Gaussian curve and red is Ca Gaussian curve.

As it can be seen in figure 2.15 above, the sum function fits well to the peak. With this we were confident that we could apply it to obtain Ca X-ray fluorescence intensity.

2.4. Statistical Analysis

Statistical analysis was achieved with Graph-Pad Prism v.5 (GraphPad Software). Data are expressed as percentages of values obtained in control conditions, and are presented as mean ± SEM. Statistical analyses were performed using the one-way ANOVA followed by Bonferroni's multiple comparison test. Values of $p<0.05$ were considered significant.

Chapter 3 - Experimental Results and Analysis

3.1. Optimization of the signal to background ratio

3.1.1. X-ray fluorescence spectrometer parameter selection

In what concerns the X-ray spectrometer parameter selection, we had to consider the acquisition time, the size of the X-ray collimator, voltage and electric current, the X-ray filter and the peaking-time of the front-end electronics. Parameter are related with each other and so the options available to choose one of them depend on what we choose to others.

The acquisition time is an important parameter because it allows to obtain more statistics for the events measured, helping to define the X-ray fluorescence peaks well above the background of the spectrometer. As we had a low counting rate for the majority of the fluorescence X-rays emitted from the atomic elements studied in this work, we choose 600 s of acquisition time after we had also tried 300 s.

The size of the collimator is the size of the X-ray beam on the sample. We had the option to choose between 0.2×0.2 mm^2, 0.5×0.5 mm^2, 1.2×1.2 mm^2 and 3.0×3.0mm^2. We thought of the first two because, as they are smaller, we could do more irradiations in each structure, but the counting rate is so small that we couldn't see almost any elements. So we had to choose between 1.2×1.2mm^2 and 3×3mm^2 and, because of the calculations described before in section 2.4.1., we opted for the first one to irradiate SN and the second to ST.

The voltage applied to the X-ray tube was chosen based on the filter selected (because the elements identification depend on the filter selected). Filter selection is explained next in section 3.1.3, but we choose to use three filter by each irradiation, filter to Cl, filter to Cr and filter to PbMap. As is explained below, the first two filters are used to excite low-Z atomic elements and, taking into account that the voltage applied determines the maximum energy of the electrons that hit the anode and therefore it determines the energy band of the X-ray leaving the tube. This energy band defines the atoms that it would be able to excite, thus it was used a voltage of 15 kV to excite the samples. In the case of filter to PbMap, we wanted to identify elements of higher Z, the transition metals, and so we opted for a voltage of 30 kV.

The electric current applied in the X-ray tube determines the number of electrons that hit the anode and so the intensity of X-rays leaving the X-ray tube. Current selection was made taking into account the dead time of the detection system, since higher currents cause an elevated dead time because the limited counting rate of the detection system . On the other hand too reduced currents compromise the signal because the amount of X-rays leaving the tube decreases too. Hereupon, we have to choose the highest possible current but that don't increase the dead time too much. Besides these factors, we had to take into account the size of the beam because, as it determines the amount of X-rays that hit the sample, in the case of to 3.0×3.0 mm^2 beam the currents had to be lower than in 1.2×1.2 mm^2 beam to kept the dead time in acceptable values ($<10\%$). This way we choose 500 μA with the filter to chloride and to PbMap and 1000 μA with filter to chromium in the case of 1.2×1.2 mm^2 collimator. For 3.0×3.0 mm^2 collimator, we opted to decrease the current to 100 μA in the case of filters to Cl and to PbMap and to 200 μA with the filter to Cr.

Relatively to the peaking-time of the front-end electronics, we could choose 1 μs or 8 μs. A peaking-time of 8 μs would be the best choice because it improves the detection system electronic noise, and thus the energy resolution (see figure 2.15 above). For 1.2×1.2 mm^2 beam we had the two options for the three filters and so we opted for 8 μs. In the case of 3.0×3.0 mm^2 beam we just had the option of 1 μs. With this large beam the operation at 8 μs is avoided due to the long time duration of the electric signals at the output of the front-end electronics, and thus provoking pile-up of the signals with the loss of its individual energy information at high counting rates.

For filter selection we had the option of no filter at all, an universal filter, a filter to Pb, a filter to PbMap, a filter to Cr and a filter to Cl. The main function of the X-ray filters is to reduce background counts in a particular energy range of the spectrometer spectra. No filter and universal filter were never an option because we couldn't identify any peak in the X-ray energy spectrum. Figure 3.1 depicts the spectra from three acquisitions with no sample, just irradiating the Perspex block with the primary X-ray beam from the X-ray tube. The point is to show the aspect of the spectrum given by each filter. As it can be seen, in figure 3.1a, the filter to Cl produces a "clean" region until ~4 keV allowing to measure atomic elements of low-Z. In Figure 3.2 b, the filter to Cr yields a spectrum where the background starts to grow for ~6 keV, allowing to measure iron. In Figure 3.1c, the filter to PbMap produces low background rate within 4–10 keV range, allowing to measure the atomic elements with fluorescence X-rays energy in this gap, such as the iron, copper and zinc.

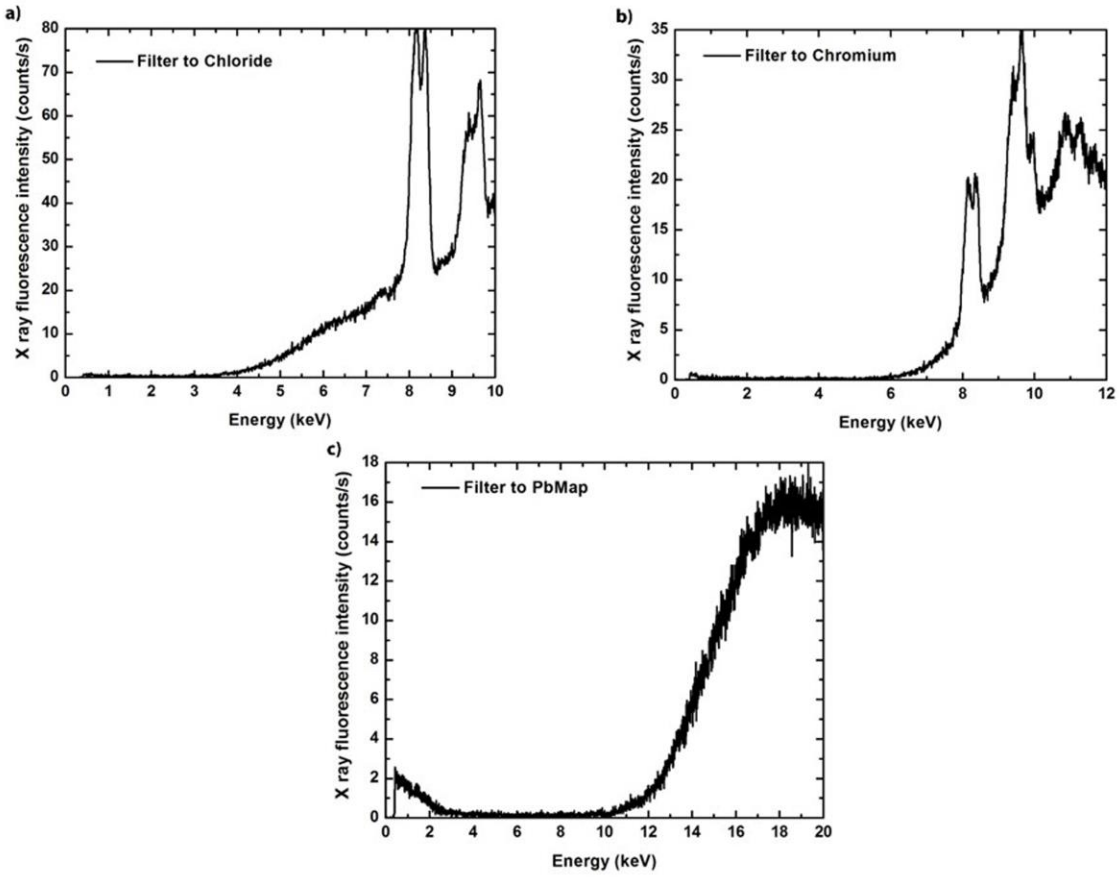

Figure 3.1 – The response of the three filters used in this work: a) filter to Cl (X-ray tube conditions: 15 kV and 500 μA); b) filter to Cr (X-ray tube conditions: 15 kV and 1000 μA); and c) filter to PbMap (X-ray tube conditions: 30 kV and 500 μA).

3.1.2. Sample thickness

First, tissue samples with 1 mm thickness (in the cut) were tested; with those we were able to see the elements phosphorus, sulfur, chloride, potassium and calcium with filter to chloride. Phosphorus, sulfur, chloride, potassium, calcium and iron with filter to chromium and iron, copper and zinc with filter to PbMap.

Nevertheless, the counting rates for the elements were low, and thus considering the anatomical characteristics of the structures that we wanted to irradiate (*substantia nigra*, SN and *striatum*, ST), we decide to cut the final samples with 3 mm of thickness. Raising the thickness of the sample, we guarantee that we had more atoms that can be excited by the primary X-rays and so the amount of fluorescence X-rays that would hit the detector and ultimately, the counting rate would increase too.

3.2. The elements fluorescence intensity in control and in treated group

3.2.1. In *substantia nigra*

Measurements in SN were performed using the parameters referred previously for each one of the three filters being common the 600 s of acquisition time and 8μs of peaking time and 1.2×1.2 mm^2 for the beam size. With the filter for chloride, the current was 500 μA and voltage 15 kV. For chromium, the current was 1000 μA and voltage 15 kV and for PbMap, was 500 μA and 30 kV.

The first spectrum (a)) of all the images presented next is an example of the graphs that we obtained for each filter, having the control, C (black line) and treated, T (red line) lines overlapping so we can observe the differences between the two groups. These results weren't treated and so represent all the counts given by the system software with no background subtraction.

For each sample we performed four measurements, so each point in the dispersion graphs presented below result from the sum of those four measurements (after the Gaussian fitting and so representing net counts/s) being the full point in each group the average of the four (in control group, C) and five (in treated group, T) empty points. In each average point it's represented an error bar (that cannot be seen in all cases because of its size in comparison with graph scale) that concerns the standard deviation of the errors of every Gaussian fittings for that group of measurements. All this graphs were done using OriginPro8 software.

First image, figure 3.2, represents spectra with the filter to Cl. As has been referred, a) represents untreated data and we can see the peak of phosphorus (P), sulfur (S), chloride (Cl), potassium (K) and calcium (Ca). Ca K_α peak is summed with K K_β and so the dashed vertical line divides the peak in the two zones. For this filter we considered an energy interval from 1.5 to 4 keV because of the K_α energies from the elements presented being inside this range. Graph b), c), d), e) and f) represent elements data.

In graphs b), c), d) and e) we can see a slight increase in, respectively, P, S, Cl and K average level of counts/s and also that the values have a considerable dispersion between each other.

Graph f), exposing Ca levels, exposes a decrease in this element average levels, from 61.74 counts/s (0.41 of error) to 59.36 counts/s (0.45 of error). It should be noted that in the case of Ca, treated group, a point was withdrawn because it was considered a significant outlier by GraphPad software.

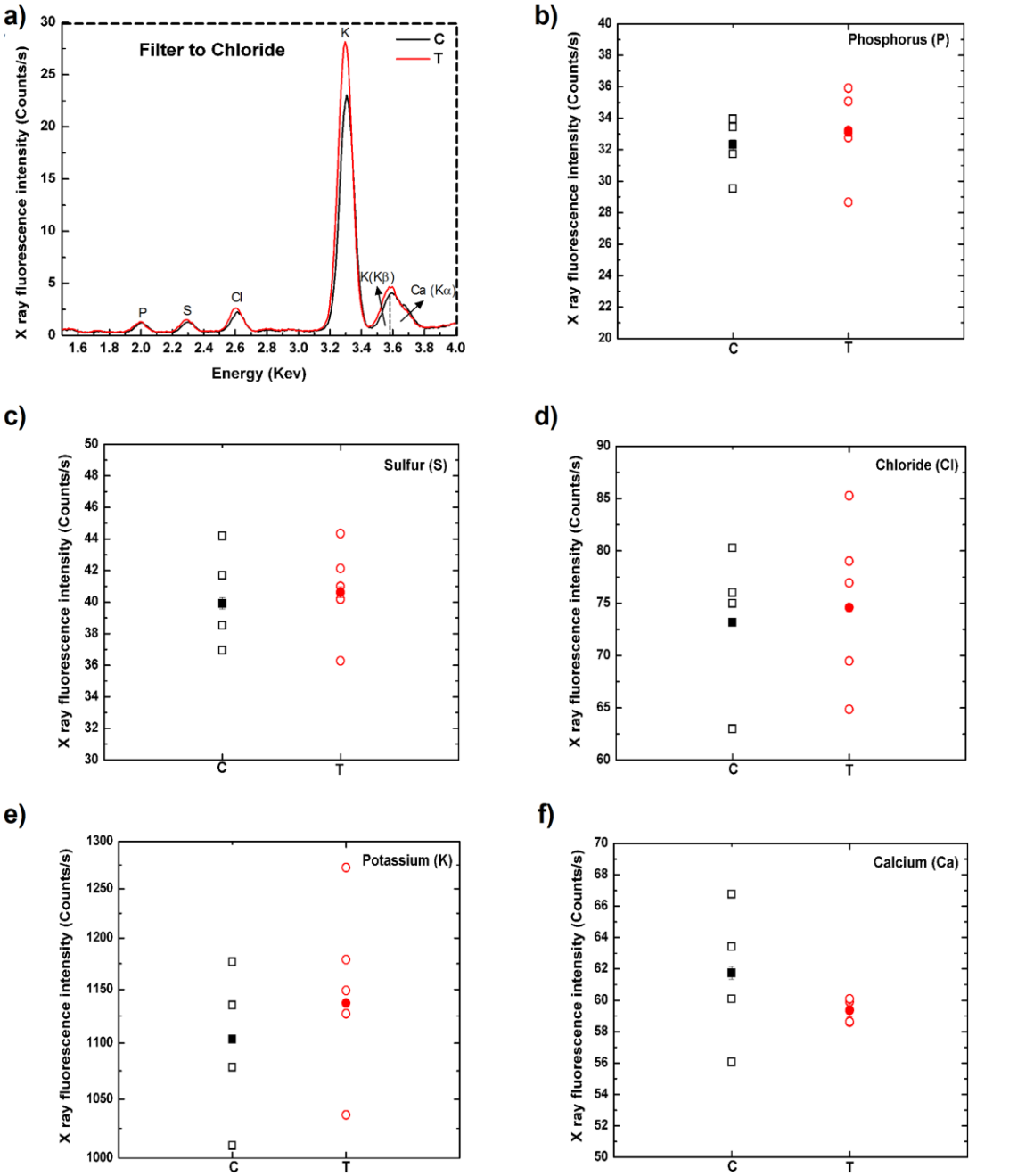

Figure 3.2 – X-ray fluorescence intensity obtained in SN using a filter to Cl. a) example of two spectra, resulting of acquisitions with an 1.2×1.2 mm^2 beam, 500 μA and 15 kV in which we can see the elements P, S, Cl, K and Ca (peak results from the sum of K_β of K and K_α of Ca and so the dashed line is dived the peak). C is for control (black) and T for treated (red), empty, squares and spots, represent a sample value of X-ray fluorescence intensity and full the average of them. b) phosphorus, c) sulfur, d) chloride, e) potassium and f) calcium.

Figure 3.3, represents data from filter to chromium. As has been referred, a) represents untreated data and we can see the peak of phosphorus (P), sulfur (S), chloride (Cl), potassium (K), calcium (Ca) and iron (Fe). Ca K_α peak is summed with K K_β and so the dashed vertical line divides the peak in the two zones. For this filter we considered an energy interval from 1.5 to 7 keV.

In graph b), f) and g) we can see a slight decrease in, respectively, P, Ca and Fe average level of counts/s and also that the values have a considerable dispersion between each other in case of phosphorus and iron and in control group of calcium. In the case of treated group of calcium, a point was withdraw because it was considered an outlier by GraphPad software.

Graph c), d) and e) show slight increases in, respectively, S, Cl and K.

In the case of graph g), the average of X-ray fluorescence intensity of iron in control group (C) is 28.60 counts/s (error of 0.4) and 25.72 counts/s (error of 0.34) for treated group (T).

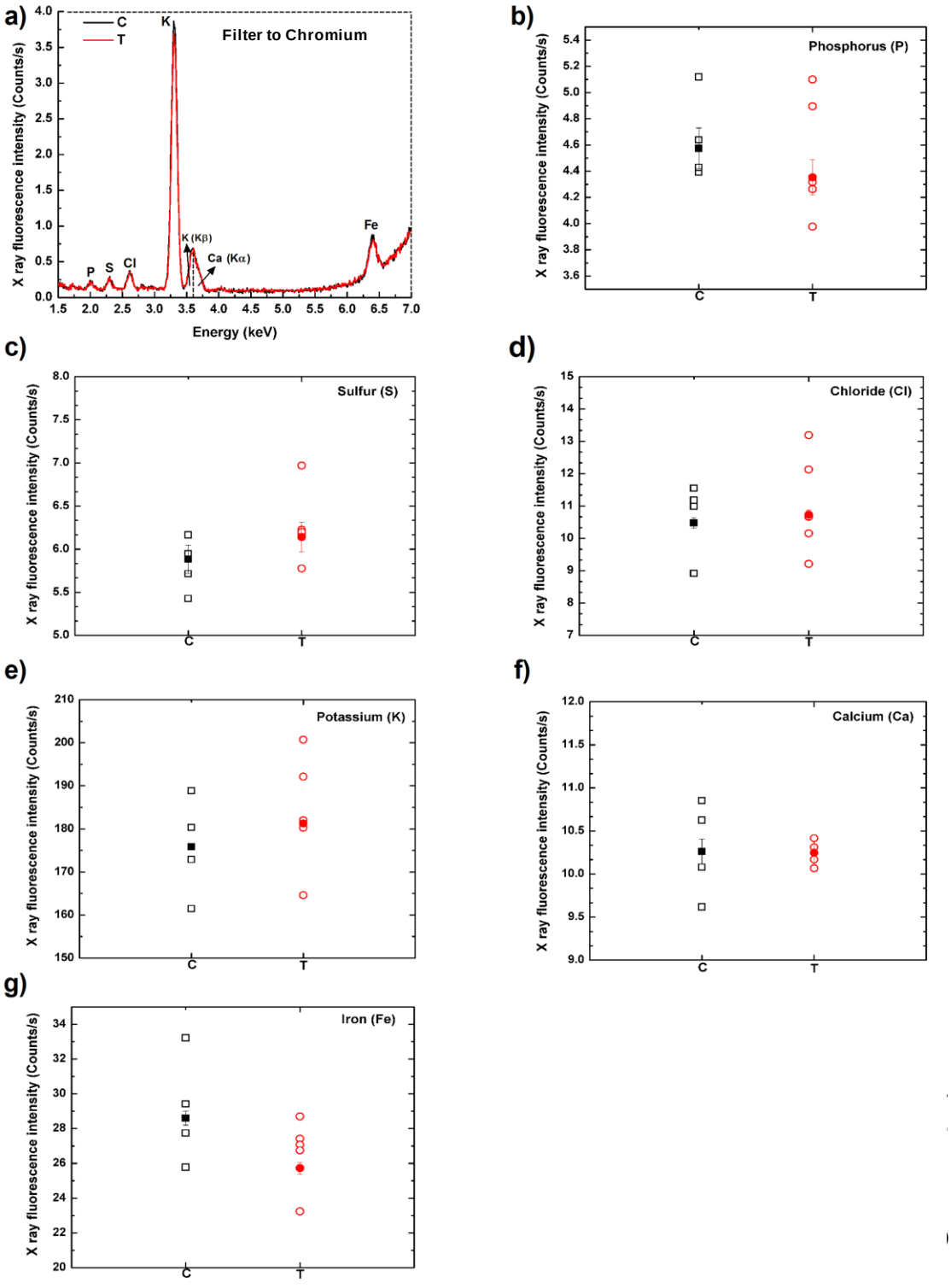

Figure 3.3 –X-ray fluorescence intensity obtained in SN using a filter to Cr. a) example of spectra, resulting of acquisitions with an 1.2×1.2 mm^2 beam, 1000 μA and 15 kV in which we can see the elements P, S, Cl, K, Ca and Fe (peak results from the sum of Kβ of K and Kα of Ca and so the dashed line is dived the peak). C is for control (black) and T for treated (red), empty, squares and spots, represent a sample value of X-ray fluorescence intensity and full the average of them. b) phosphorus, c) sulfur, d) chloride, e) potassium, f) calcium and g) iron.

Figure 3.4 shows data from SN irradiations using filter to PbMap. As has been referred, a) represents the spectra and we can see the peak iron (Fe), copper (Cu) and zinc (Zn). For this filter we considered an energy interval from 6 to 9keV because of the K_α energies from the elements presented being inside this range (K_α of iron is 6.4 keV, copper is 8.042 keV and 8.631 keV for zinc).

Graph b) represents iron X-ray fluorescence intensity and we can see that the average is slightly increased in the control group, from 6.99 counts/s (error of 0.17) to 7.09 counts/s (error of 0.15).

Zinc, in graph d) is decreased from 13.74 counts/s (0.18 of error) in control group to 13.24 counts/s (0.17 error) in treated group.

In the three graphs the values have a considerable dispersion between each other except in zinc control group. In the case of treated group of iron, a point was withdraw because it was considered an outlier by GraphPad software.

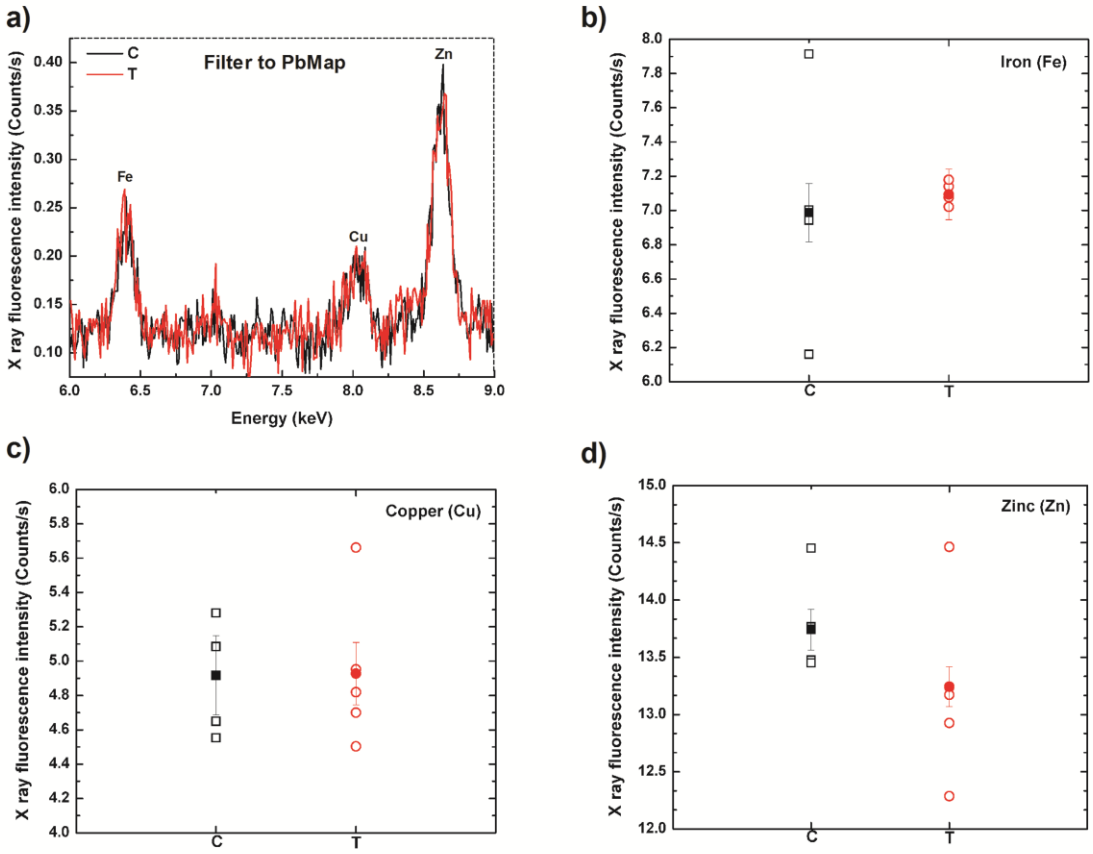

Figure 3.4 – X-ray fluorescence intensity obtained in SN using a filter to PbMap. a) example of two spectra, resulting of acquisitions with an 1.2×1.2 mm^2 beam, 500 μA and 30 kV in which we can see the elements Fe, Cu and Zn. C is for control (black) and T for treated (red), empty, squares and spots, represent a sample value of X-ray fluorescence intensity and full the average of them. b) iron, c) copper and d) zinc.

3.2.2. In *striatum*

Measurements in ST were performed using the parameters referred previously for each one of the three filters being common the 600 seconds of acquisition time and 1 μsec of peaking time and 3.0×3.0 mm^2 for the beam size. About filter for chloride, the current was 100 μA and voltage 15 kV. For chromium, 500 μA and 15 kV and for PbMap, 100 μA and 30 kV.

Similar to what has been said in the case of SN measurements, the first graph (a)) of all the images presented next is an example of the spectra that we obtained for each filter, C represents the control and has the black line and the red one is for treated group (T).

Measurements in ST were performed the same way the ones in SN, so the following graphs have the same organization shown before. For each sample we performed four measurements, so each point in the dispersion graphs presented below result from the sum of those four measurements (after the Gaussian fitting and so representing liquid counts/s) being the full point in each group the average of the four (in control group, C) and five (in treated group, T) empty points. In each average point it's represented an error bar (that cannot be seen in all cases because of its size in comparison with graph scale) that concerns the standard deviation of the errors of every Gaussian fittings for that group of measurements. All this graphs were done using OriginPro8 software.

First image, figure 3.5, represents data from filter to Cl. As has been referred, a) represents untreated data and we can see the peak of phosphorus (P), sulfur (S), chloride (Cl), potassium (K) and calcium (Ca). Ca K_α peak is summed with K K_β and so the dashed vertical line divides the peak in the two zones. For this filter we considered an energy interval from 1.5 to 4 keV because of the K_α energies from the elements presented being inside this range. Graph b), c), d), e) and f) represent elements data.

All the graphs (from b) to f)) show slight decreases in X-ray fluorescence intensity. In the case of Ca, for example, the diminution is from 70.32 counts/s (error of 0.52) in the control group to 67.30 counts/s (error of 0.45) to treated group.

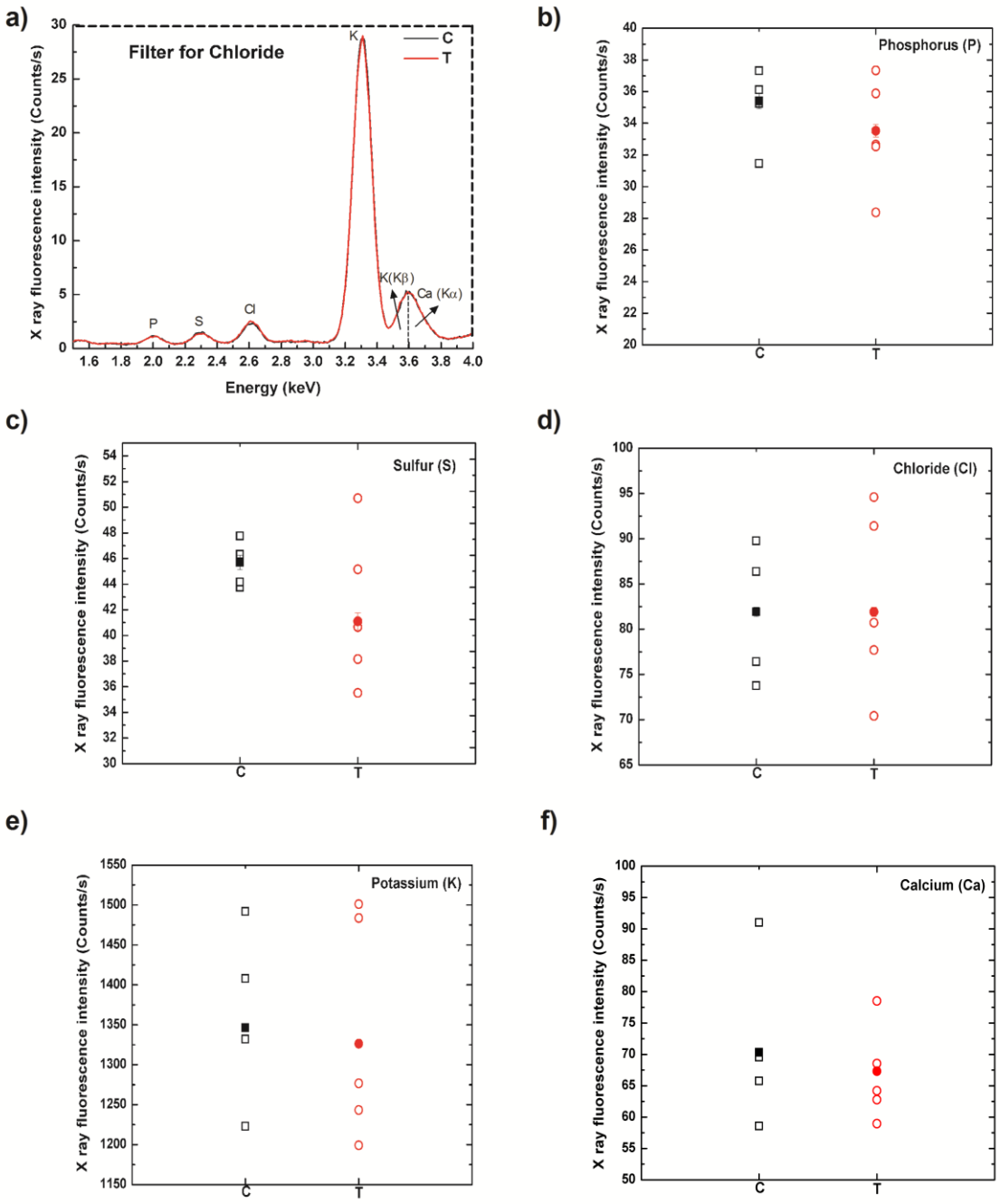

Figure 3.5 – X-ray fluorescence intensity obtained in ST and using a filter to Chloride. a) example of two spectra, resulting of acquisitions with an 3.0×3.0 mm^2 beam, 100 μA and 30 kV in which we can see the elements P, S, Cl, K and Ca. C is for control (black) and T for treated (red), empty, squares and spots, represent a sample value of X-ray fluorescence intensity and full the average of them. b) phosphorus, c) sulfur, d) chloride, e) potassium and f) calcium.

Figure 3.6, represents data from filter to chromium acquired in ST. As has been referred, a) represents the spectra with the peak of phosphorus (P), sulfur (S), chloride (Cl), potassium (K), calcium (Ca) and iron (Fe). Ca K_α peak is summed with K K_β and so the dashed vertical line divides the peak in the two zones.

In graphs b), e), f) and g) we can see a slight decrease in, respectively, P, K, Ca and Fe average level of counts/s and also that the values have a considerable dispersion between each other. In the case of treated group of sulfur and calcium, a point was withdraw because it was considered an outlier by GraphPad software.

Graphs c) and d) show slight increases in, respectively, S and Cl.

In the case of graph g), the average of X-ray fluorescence intensity of iron in control group (C) is 28.60 counts/s (error of 0.4) and 25.72 counts/s (error of 0.34) for treated group (T).

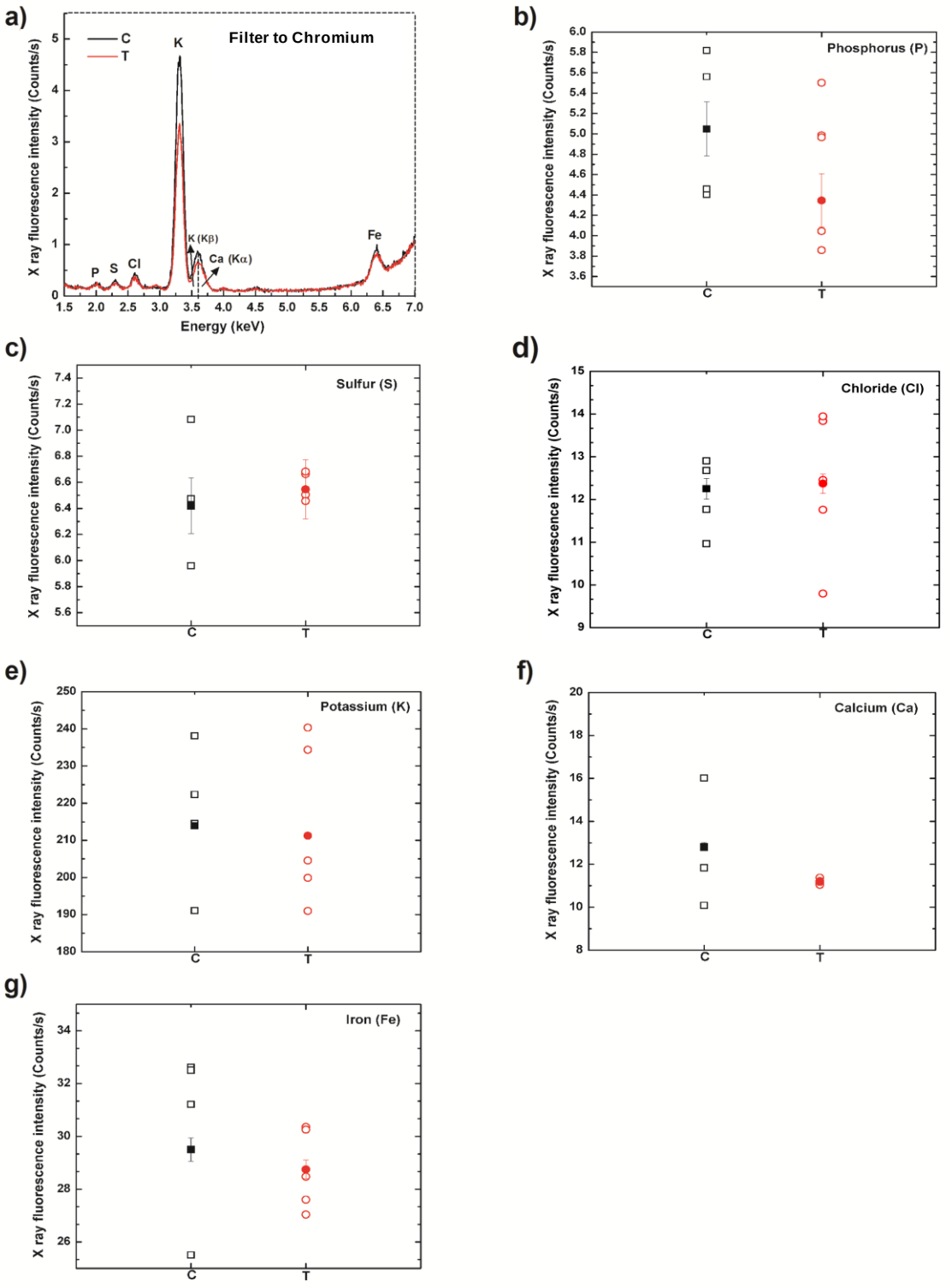

Figure 3.6 – X-ray fluorescence intensity obtained in ST using a filter to chromium. a) example of two spectra, resulting of acquisitions with an 3.0×3.0 mm^2 beam, 200 μA and 15 kV in which we can see the elements P, S, Cl, K, Ca and Fe (peak results from the sum of Kβ of K and Kα of Ca and so the dashed line is dived the peak). C is for control (black) and T for treated (red), empty, squares and spots, represent a sample value of X-ray fluorescence intensity and full the average of them. b) phosphorus, c) sulfur, d) chloride, e) potassium, f) calcium and g) iron.

Figure 3.7 shows data from ST irradiations using filter to PbMap. As has been referred, a) represents spectra with the peak iron (Fe), copper (Cu) and zinc (Zn).

Graph b) represents iron X-ray fluorescence intensity and we can see that the average is slightly increased in the control group, from 8.13 counts/s (error of 0.17) to 8.37 counts/s (error of 0.19).

Cu, in graph c) shows an increased average in treated group of 6.39 (0.23 error) compared with 5.38 in controls.

Zn, in graph d) is decreased from 19.89 counts/s (0.21 of error) in control group to 18.87 counts/s (0.23 error) in treated group.

In the three graphs the values have a considerable dispersion between each other.

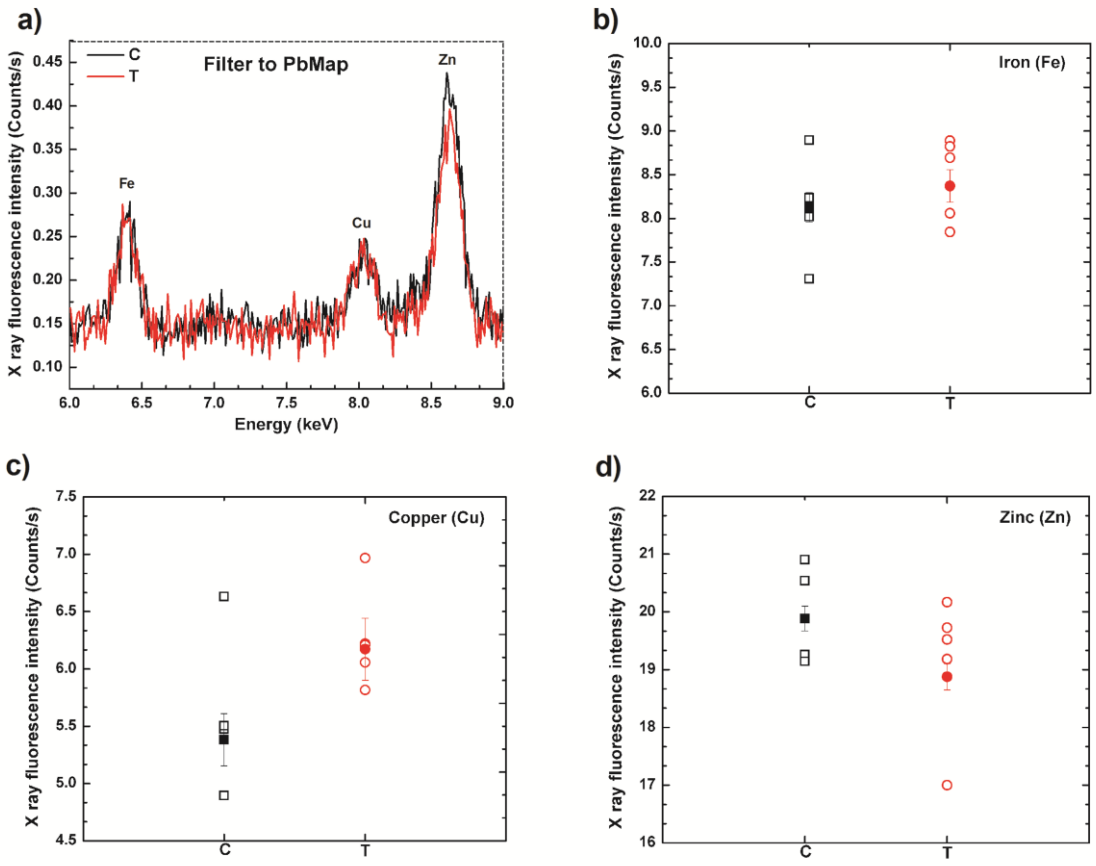

Figure 3.7 – X-ray fluorescence intensity obtained in ST and using a filter to PbMap. a) example of two spectra, resulting of acquisitions with an 3.0×3.0 mm^2 beam, 100 μA and 30 kV in which we can see the elements Fe, Cu and Zn. C is for control (black) and T for treated (red), empty, squares and spots, represent a sample value of X-ray fluorescence intensity and full the average of them. b) iron, c) copper and d) zinc.

3.3. Comparison between the two groups

3.3.1. In *substantia nigra*

To better compare the two groups, control (C) and treated (T) we made a statistical analysis for all the elements in each filter using one way ANOVA test and Bonferroni as post test to determine statistical significance. The statistical analysis was performed with GraphPad Prism v.5 (GraphPad Software Inc., San Diego CA). Data are expressed as percentage of values obtained in controls conditions and presented as mean ± SEM. Values of $p<0.05$ were considered statistically signaificant.

Figure 3.8 represents the acquisitions in *substantia nigra* (SN). In Figure 3.8 a) is represented the analysis of data resultant of the acquisitions with filter for Cl where we can see P, S, Cl, K and Ca represented in percentage of controls. We can observe a tendency to increase in all elements except for Ca (3.693 ± 0.6544%), being the differences not statistically significant.

In Figure 3.8 b) we can see data from the acquisitions using filter for Cr, representing percentage of controls of P, S, Cl, K, Ca and Fe. P, Ca and Fe decrease and S, Cl and K increase. As in the case of filter to Cl, there wasn't any difference that was considered statistically significant but, for example, in the case of iron the mean difference was 8.395 ± 1.413%.

The Figure 3.8 c) represents the filter to PbMap. The percentage of control increases in the case of Fe and Cu and decrease for Zn. In this case statistical analysis didn't considered any of the mean different. In the case of Fe 1.424 ± 0.2907%, Cu 0.7209 ± 0.1551% and for Zn 4.133 ± 0.8894%.

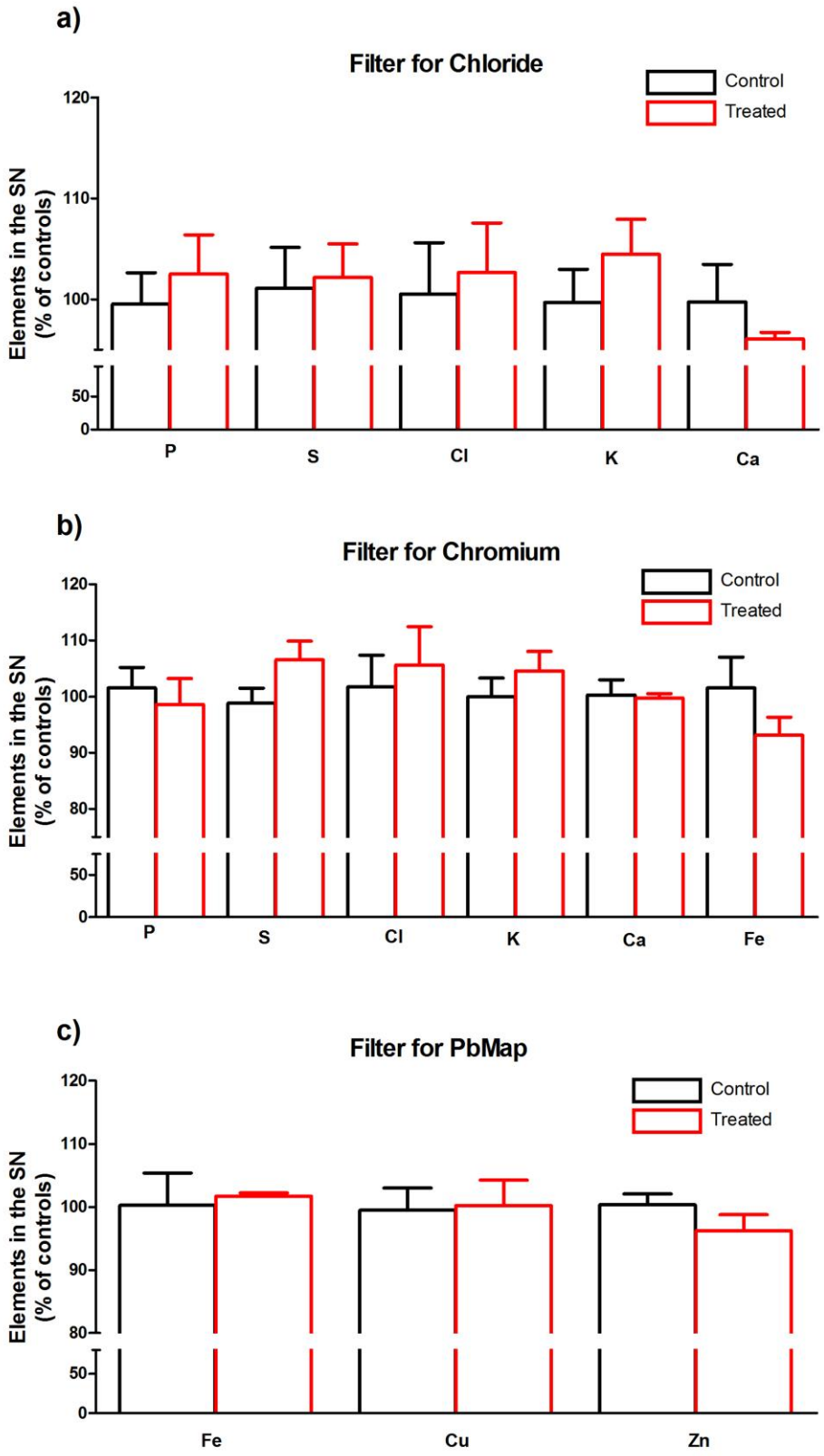

Figure 3.8 - Elements in SN in percentage of control. a) filter to Cl, b) filter to Cr and c) filter to PbMap.

3.3.2. In *striatum*

In the case of ST measurements, we have performed the statistical analysis as described above for the SN. In Figure 3.9 a) is represented the statistical analysis of the data resultant from irradiations using filter to Cl where we can observed P, S, Cl, K and Ca. In all elements there was a decrease in percentage of controls except for Cl. Analyzing all these elements there wasn't any statistical difference between the two groups, but, for example, in the case of Ca the mean difference was 6.583 ± 0.8981%.

Figure 3.9 b) shows the data from filter to Cr, representing percentage of controls of P, S, Cl, K, Ca and Fe. In this filter we can observe an increase in S and Cl and a decrease in P, K, Ca and Fe. As in the case of filter to Cl, there wasn't any statistical difference between the two groups. Nevertheless, for example, in the case of Fe the mean difference was 5.797 ± 0.7895% and Ca 11.69 ± 1.511%. It has to be mentioned that in calculation of S and Ca there was a point withdraw in the control group of both because it was considered an outlier, which was calculated using the outlier calculator from GraphPad Software.

Graph c) represents the filter for PbMap. There is visible here an increase in Fe and Cu and a decrease in Zn. In this case the statistical analysis didn't considered the mean differences of the two groups statistically different. The obtained means were for Fe 4.276 ± 0.8191%, and for Zn 4.235 ± 0.8112%. In the case of Cu there was a statistical significant increase of 15.53 ± 2.974% in the treated group as compared with the controls.

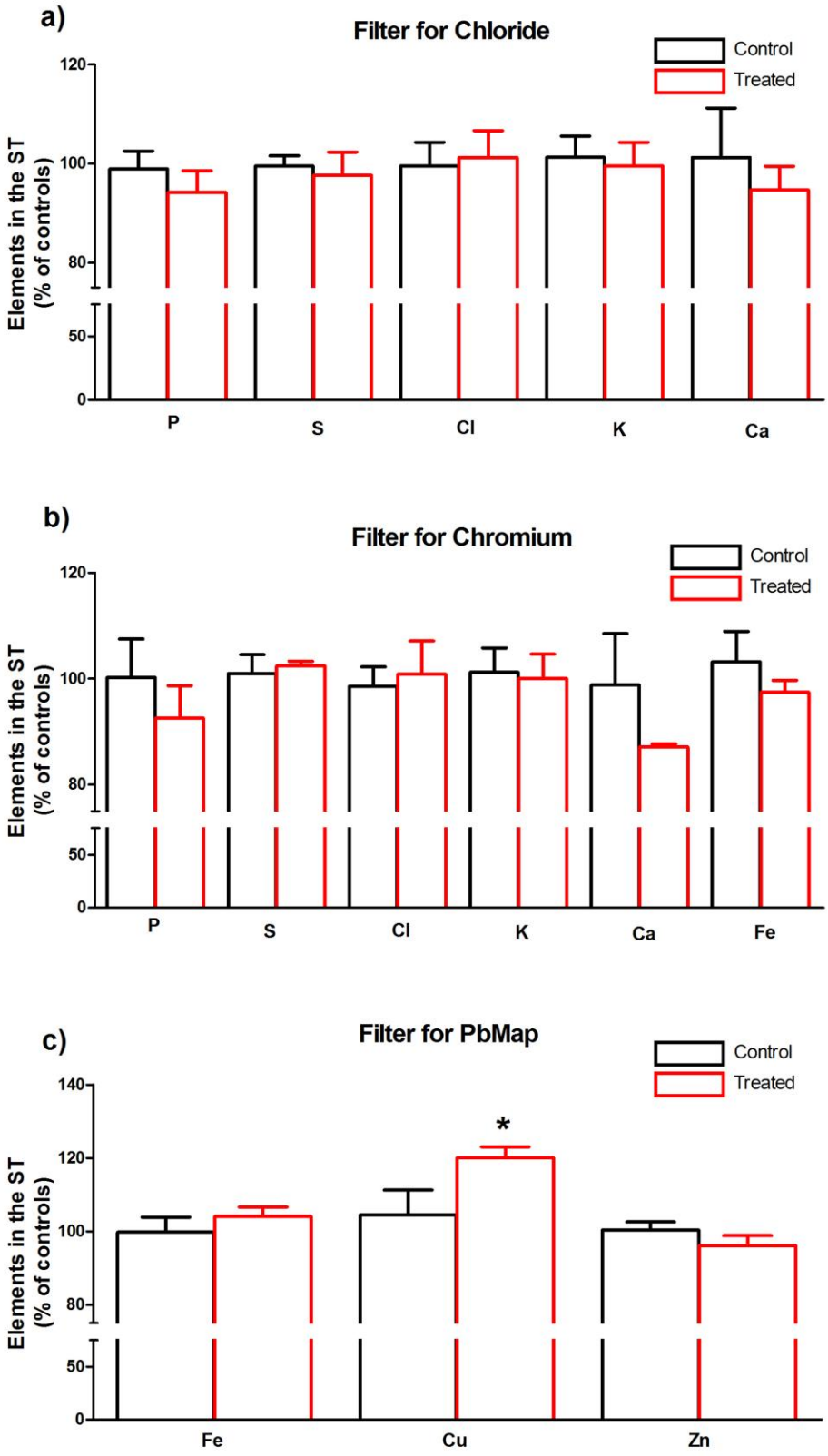

Figure 3.9 - Elements in ST in percentage of control. a) filter to Cl, b) filter to Cr and c) filter to PbMap.

Chapter 4 – Discussion

Present work is, of what we know, the first one that use X-ray fluorescence intensity to identify elements in a Parkinson's disease (PD) model induced by paraquat (PQ). To do this identification we used the X-ray fluorescence spectrometer SEA6000VX from Hitachi High-Tech Science Corporation. As it was no documentation of an experiment like this, the first step was to optimize the conditions of operation of the spectrometer.

This optimization was made taking in account some physic principals and, some parameters, by trial and error. The first challenge we faced was the sample thickness. The first attempt samples were of 1 mm but, considering the low count rate at which we were working and the anatomical characteristics of the brain zones we wanted to analyze, we have chosen 3 mm samples and from there we obtained well defined X-rays fluorescence peaks for the several elements analyzed.

The next step was to select the X-ray tube parameters that better served our purpose. First, we had to explore all the possibilities of time of measurement, voltage, current, collimator (beam size), filter, environment and peaking time. In terms of time of measurement, we have chose 600 seconds because we had to give the system enough time to construct the peaks but we also had to consider the thawing of the samples and the resources spent.

Collimator size was chosen based on the size of the structures that we were going to analyze and so, in the case of SN samples had 1.2×1.2 mm^2 and ST, 3.0×3.0 mm^2.

Voltage, current and filter selection was made by trial and error with the purpose of obtain the best signal to background ratio (SBR) possible since the system had some restrictions in the combinations. Whereupon, we choose 15 kV for filter to chloride and 500 μA because it was the best option available. In the case of filter to chromium we had the option to choose 1000 μA with the same 15 kV and so we opted for this current because the more power is supplied, the higher the excitation in the sample. Finally, in the case of filter to PbMap, as the objective was the excitation of higher Z elements, the option of 30 kV was available and we choose it with 500 μA of current being the best possibility. The physics fundamentals that justify these choices are exposed before in section 3.1.1 and 3.1.2.

In what concerns the samples irradiation environment, from the beginning we thought that using He purge was the best option because in this way we won't have an argon peak cover the region of low-Z elements and He has a very low atomic number thus cannot be detected by the detection system, and in this way does not interfere with our measurements.

The peaking time used was 8 μs by default and showed to be the best solution (higher peaking time, higher peak definition, as explained before in section 3.1.1) but in the case of 3.0×3.0 mm^2 beam the system did not allow this choice and so, in this case we had to choose 1 μs.

At the end we achieved a good signal to background ratio and we were able to identify several elements (phosphorus, sulfur, chloride, potassium, calcium, iron, copper and zinc). With this setup we were able to measure elements that we did not expect to measure, such as, phosphorus, sulfur, chloride and potassium, as referred above. We didn't expect to see these elements because they have a low Z and also because they are not documented as determinant in PD pathology.

After the analysis of the results, we were not able to establish a connection between the variations of phosphorus, sulfur and potassium in the two groups (control and treated) and the two brain regions (*substantia nigra* (SN) and *striatum* (ST)). With regard to other elements (chloride, calcium, iron, copper and zinc), although no statistical significance were observed (except in the case of copper values measured in ST), a pattern could be established.

Starting with chloride, we can see that it is augmented in both SN and ST using the filter to chloride and the filter to chromium. There is no evidence of this increase to be related to PD and so we speculate that it could be an effect resultant from the use of paraquat (PQ). The PQ chemical formula is 1,1-dimethyl-4,4'-bipyridinium dichloride [53] and so its injection may have increased the quantity of this element in the brains of the treated group. There is a study that states that the increased content of chloride in PD brains is responsible for the inhibition of some enzymes involved on dopamine formation leading to the decrease of this neurotransmitter [61].

In the case of calcium, there was a non-significant decrease in the X-rays fluorescence of this element in both SN and ST, when using the filter to chloride and the filter to chromium. Calcium is a very important element in the brain being involved in many different intracellular and extracellular processes as synaptic activity, cell communication and memory formation [62]. A recent work states that disturbance of the intracellular calcium homeostasis may provide part of an adverse outcome pathway that connects pesticide exposure with neurodegeneration [63]. It was also showed that calcium levels are different between PD patients and healthy persons, which suggest that disturbances of calcium homeostasis may be linked to PD [64] and, more recently, that malfunction of some enzymes dependent of calcium can be the key factor for motor symptoms in PD [65]. Furthermore, it has been suggested that the toxicity of PQ is related with the inhibition of mitochondrial respiratory chain and to cycling of one-electron transport from NADH to an oxygen molecule. This process leads to production of toxic reactive oxygen species and to an energy crisis [54]. Severe defects in complex I activity are assumed to depress ATP synthesis, induce mitochondria

depolarization, and favor calcium deregulation [55]. Mitochondria is involved in calcium homeostasis because it is able to uptake calcium, reducing its concentration in the cytosol and, with the appropriate stimulus, is able to release calcium content through a Na+/Ca2+ exchanger and the mitochondrial permeability transition pore. The extended opening of this pore leads to the release of apoptotic factors and cell death [62].

In the case of iron, the results obtained with the two filters are not the same. Using the filter to chromium iron X-ray fluorescence intensity decreases in both SN and ST and when using the filter to PbMap iron values increased. As it has been referred before in the introduction, it was previously observed that patients with PD tend to accumulate iron in their nervous system [2, 3, 5, 7, 22, 23, 25, 26, 28, 29, 37, 41-44], suggesting a role for this transition metal in this disorder. Iron is a transition metal and participates in Fenton reaction which may cause damage to neurons, by the production of reactive oxygen species (ROS). It is not surprising that in the SN and other dopaminergic regions, high levels of iron could play an important role in the loss of dopaminergic neurons [26, 29]. Although the observed changes were not statistically significant the small increases (1% in SN and 4% in ST) observed with the filter to PbMap are consistent with reports previously published unlike the results obtained using the filter to chromium.

For copper X-ray fluorescence intensity especially in the ST we found a statistical increase of 15% of this element in the treated group when compared with the control. As mentioned in the introduction, it is known that copper has a dual effect in the brain. It can increase oxidative stress by participating in Fenton reaction [29] or can help fighting this condition by acting has a co-factor of the antioxidant enzyme, superoxide dismutase (SOD) [30]. It is known that PQ releases transition metal from metalloproteins storage [53], so it is possible that in our model, after the administration of PQ, a similar process may be responsible for the increased concentration of copper in the ST, giving rise to oxidative processes leading to neuronal toxicity. Moreover, it is known that copper ions plays a role in the pathogenesis of PD. This role as been associated with copper ion ability to form a complex with the above mentioned cytosolic protein α-synuclein (α-syn), which forms insoluble aggregates (so called Lewy bodies, LB) localized in the brain dopaminergic neurons in patients with PD. Thus, copper is an important factor promoting the folding of α-Syn into neurotoxic aggregates. [49]. In summary, the increase of copper is, probably, contributing to PD pathogenesis by raising ROS levels by Fenton reaction, by increasing α-Syn aggregation forming LB and by decreasing the antioxidant power by saturation SOD.

Zinc X-ray fluorescence was shown to be decreased in both SN and ST. There is a previous study that states that the ratio of zinc and copper must be in relative balance for the two trace elements to act as an antioxidant. An excess of copper can cause a relative zinc deficiency, reducing SOD activity [66]. Maintaining of Zn and Cu homeostasis in the brain is

extremely important, and deviations from it can be fatal for neurons [49]. An insufficiency of copper and zinc also can induce oxidative stress because it results in a decrease in the superoxide dismutase activity, which is an important component of the organism's antioxidant defense [49].

Summarizing, taking into account the results obtained with the filter to PbMap, Fe and Cu are increased contributing to the production of ROS and consequent damage of dopaminergic neurons. And Zn, responsible for immune response in the brain, is decreased contributing to a deficient immune defense and so to more damage in these tissues.

Chapter 5 – Conclusions and Future Work

This work is an attempt of an elementary characterization of a Parkinson's disease (PD) model using a commercial non-dedicated X-ray fluorescence spectrometer. This characterization was achieved because we identify several elements but we didn't recorded statistical significant differences (between the two groups, control and treated) in the measurements performed except in the case of copper in striatum (ST).

To do this identification we optimize the conditions for each brain zone and for each filter used and these conditions can now be used in future studies using this system and biological samples.

This work used a model of Parkinson's disease (PD) induced by paraquat (PQ). There was no evidence that this model causes directly variations in metal amounts and so maybe the almost no differences that we observed in this study are due to the model. Thus, try to use another PD model can be an option.

In terms of samples, we have seen a considerable dispersion between values inside the same group. This may be related to the reduced number of samples (4 controls and 5 treated) and so increase these numbers in a next experiment may decrease the statistical error.

Bibliography

[1] Lawerence M Sayer, George Perry, Mark A Smith, "Redox metals and neurodegenerative disease," *Current Opinion in Chemical Biology,* vol. 3, pp. 220-225, 1999.

[2] K. A. Jellinger, "The relevance of metals in the pathophysiology of neurodegeneration, pathological considerations," in *International Review of Neurobiology*. vol. 110, 1 ed: Elsevier Inc., 2013, pp. 1-47.

[3] V. N. Uversky, J. Li, and A. L. Fink, "Metal-triggered structural transformations, aggregation, and fibrillation of human alpha-synuclein. A possible molecular NK between Parkinson's disease and heavy metal exposure," *The Journal of biological chemistry,* vol. 276, pp. 44284-96, 2001.

[4] B. F. G. Popescu and H. Nichol, "Mapping brain metals to evaluate therapies for neurodegenerative disease," *CNS neuroscience & therapeutics,* vol. 17, pp. 256-68, 2011.

[5] G. Hebbrecht, W. Maenhaut, and J. D. Reuck, "Brain trace elements and aging," *Nuclear Instruments and Methods in Physics Research Section B: Beam Interactions with Materials and Atoms,* vol. 150, pp. 208-213, 1999.

[6] Youdim MB, Ben-Shachar D, Riederer P, "Is Parkinson's disease a progressive siderosis of substantia nigra resulting in iron and melanin induced neurodegeneration?," *Acta Neurol Scand Suppl,* vol. 126, pp. 47-54, 1989.

[7] M. W. Bourassa and L. M. Miller, "Metal imaging in neurodegenerative diseases," vol. 4, ed. Metallomics, 2012, pp. 721-738.

[8] D. Hare, B. Reedy, R. Grimm, S. Wilkins, I. Volitakis, J. L. George, *et al.*, "Quantitative elemental bio-imaging of Mn, Fe, Cu and Zn in 6-hydroxydopamine induced Parkinsonism mouse models," *Metallomics,* vol. 1, pp. 53-58, 2009.

[9] D. J. V. Junjing Deng, Si Chen "Simultaneous cryo X-ray ptychographic and fluorescence microscopy of green algae.," *PNAS,* vol. 112, pp. 2314-2319, 2014.

[10] T. Paunesku, S. Vogt, J. Maser, B. Lai, and G. Woloschak, "X-ray fluorescence microprobe imaging in biology and medicine," *J Cell Biochem,* vol. 99, pp. 1489-502, 2006.

[11] C. J. Fahrni, "Biological applications of X-ray fluorescence microscopy: exploring the subcellular topography and speciation of transition metals," *Current Opinion in Chemical Biology,* vol. 11, pp. 121-7, 2007.

[12] P. A. Mandò, "PIXE (Particle-Induced X-Ray Emission)," in *Encyclopedia of Analytical Chemistry*, R. A. Meyers, Ed., ed: John Wiley & Sons, Ltd, 2006.

[13] F. Lin, I. M. Markus, M. M. Doeff, and H. L. Xin, "Chemical and structural stability of lithium-ion battery electrode materials under electron beam," *Scientific Reports,* vol. 4, pp. 1-6, 2014.

[14] N. Masaki, I. Ishizaki, T. Hayasaka, G. L. Fisher, N. Sanada, H. Yokota, *et al.*, "Three-Dimensional Image of Cleavage Bodies in Nuclei Is Configured Using Gas Cluster Ion Beam with Time-of-Flight Secondary Ion Mass Spectrometry," *Scientific Reports,* vol. 5, pp. 1-10, 2015.

[15] C. S. Investigations. (2015, Nov). *Electromagnetic Spectrum*. Available: http://www.ces.fau.edu/nasa/module-2/radiation-sun.php

[16] B. K. Burkhard Beckhoff, Norbert Langhoff, Reiner Wedell, Helmut Wolff, *Handbook of practical X-ray fluorescence analysis.*: Springer, 2006.

[17] *Operation Manual SEA6000VX*: Hiatachi High-Tech Science Corporation, 2013.

[18] Gerald R. Lachance, Fernand Claisse, *Quantitative X-Ray Fluorescence Analysis: theory and application*: Wiley, 1995.

[19] T. Dučić, E. Barski, M. Salome, J. C. Koch, M. Bähr, and P. Lingor, "X-ray fluorescence analysis of iron and manganese distribution in primary dopaminergic neurons," *Journal of neurochemistry,* vol. 124, pp. 250-61, 2013.

[20] N. J. Jr. (2006, Dec). *Physical Principles of Ionizing Radiation*. Available: https://www.ceessentials.net/article2.html

[21] S. Takahashi, S. Hatashita, Y. Taba, X.-Z. Sun, Y. Kubota, and S. Yoshida, "Determination of the spatial distribution of major elements in the rat brain with X-ray fluorescence analysis," *Journal of Neuroscience Methods,* vol. 100, pp. 53-62, 2000.

[22] S. Yoshida, A. Ide-ektessabi, and S. Fujisawa, "Application of Synchrotron Radiation in Neuromicrobiology : Role of Iron in Parkinson ' s Disease," vol. 14, pp. 85-95, 2003.

[23] G. Robison, T. Zakharova, S. Fu, W. Jiang, R. Fulper, R. Barrea, *et al.*, "X-ray fluorescence imaging: a new tool for studying manganese neurotoxicity," *PloS one,* vol. 7, pp. e48899-e48899, 2012.

[24] D. T. Dexter and P. Jenner, "Parkinson disease: from pathology to molecular disease mechanisms," *Free radical biology & medicine,* vol. 62, pp. 132-44, 2013.

[25] D. Kaur and J. K. Andersen, "Ironing out Parkinson ' s disease : is therapeutic treatment with iron chelators a real possibility ?," *Aging Cell,* vol. 1, pp. 17-21, 2002.

[26] T. Tarohda, Y. Ishida, K. Kawai, M. Yamamoto, and R. Amano, "Regional distributions of manganese, iron, copper, and zinc in the brains of 6-hydroxydopamine-induced parkinsonian rats," *Analytical and bioanalytical chemistry,* vol. 383, pp. 224-34, 2005.

[27] J. Meiser, D. Weindl, and K. Hiller, "Complexity of dopamine metabolism," *Cell communication and signaling : CCS,* vol. 11, pp. 34-34, 2013.

[28] S. Bharath, M. Hsu, D. Kaur, S. Rajagopalan, and J. K. Andersen, "Glutathione, iron and Parkinson's disease," *Biochemical Pharmacology,* vol. 64, pp. 1037-1048, 2002.

[29] H. Kozlowski, M. Luczkowski, M. Remelli, and D. Valensin, "Copper, zinc and iron in neurodegenerative diseases (Alzheimer's, Parkinson's and prion diseases)," *Coordination Chemistry Reviews,* vol. 256, pp. 2129-2141, 2012.

[30] P. A. Kocatu, M. C. Akbostanci, and F. Tan, "Superoxide dismutase activity and zinc and copper concentrations in Parkinson ' s disease," vol. 7, pp. 63-67, 2000.

[31] O. Arias-Carrion, "Basic mechanisms of rTMS: Implications in Parkinson's disease," *Int Arch Med,* vol. 1, pp. 1-8, 2008.

[32] P. Muñoz, S. Huenchuguala, I. Paris, and J. Segura-Aguilar, "Dopamine oxidation and autophagy," *Parkinson's disease,* vol. 2012, pp. 1-13, 2012.

[33] Bender A, Desplats P, Spencer B, Rockenstein E, Adame A, Elstner M., "TOM40 mediates mitochondrial dysfunction induced by alpha-synuclein accumulation in Parkinson's disease," *PLoS One,* vol. 8, pp. 1-11, 2013.

[34] C. W. Shults, "Lewy Bodies," *Proc Natl Acad Sci USA,* vol. 103, pp. 1661-1668, 2006.

[35] R. Giráldez-Pérez, M. Antolín-Vallespín, M. Muñoz, and A. Sánchez-Capelo, "Models of a-synuclein aggregation in Parkinson's disease," *Acta neuropathologica communications,* vol. 2, pp. 176-176, 2014.

[36] E. V. Mosharov, K. E. Larsen, E. Kanter, K. A. Phillips, K. Wilson, Y. Schmitz, *et al.*, "Interplay between cytosolic dopamine, calcium, and alpha-synuclein causes selective death of substantia nigra neurons," *Neuron,* vol. 62, pp. 218-29, 2009.

[37] K. M. Davies, S. Bohic, A. Carmona, R. Ortega, V. Cottam, D. J. Hare, *et al.*, "Copper pathology in vulnerable brain regions in Parkinson's disease," *Neurobiology of aging,* vol. 35, pp. 858-66, 2014.

[38] J. Blesa and S. Przedborski, "Parkinson's disease: animal models and dopaminergic cell vulnerability," *Front Neuroanat,* vol. 8, pp. 1-12, 2014.

[39] R. F. B. Serpa, E. F. O. de Jesus, M. J. Anjos, M. G. T. do Carmo, S. Moreira, M. S. Rocha, *et al.*, "Elemental concentration analysis in brain structures from young, adult and old Wistar rats by total reflection X-ray fluorescence with synchrotron radiation," *Spectrochimica Acta Part B: Atomic Spectroscopy,* vol. 61, pp. 1205-1209, 2006.

[40] Liu G, Zhang C, Yin J, Li X, Cheng F, Li Y, "a-Synuclein is differentially expressed in mitochondria from different rat brain regions and dose-dependently down- regulates complex I activity," *Neuroscience Letters,* vol. 454, pp. 187-192, 2009.

[41] P. Ramos, A. Santos, N. R. Pinto, R. Mendes, T. Magalhães, and A. Almeida, "Iron levels in the human brain: a post-mortem study of anatomical region differences and age-related changes," *Journal of trace elements in medicine and biology : organ of the Society for Minerals and Trace Elements (GMS),* vol. 28, pp. 13-7, 2014.

[42] C. Hidalgo and M. T. Núñez, "Calcium, iron and neuronal function," *IUBMB life,* vol. 59, pp. 280-5, 2007.

[43] Y. He, "Increased iron in the substantia nigra of 6-OHDA induced parkinsonian rats: a nuclear microscopy study," *Brain Research,* vol. 735, pp. 149-153, 1996.

[44] J. Chwiej, D. Adamek, M. Szczerbowska-Boruchowska, A. Krygowska-Wajs, S. Wojcik, G. Falkenberg, *et al.*, "Investigations of differences in iron oxidation state inside single neurons from substantia nigra of Parkinson's disease and control patients using the micro-XANES technique," *Journal of biological inorganic chemistry : JBIC : a*

publication of the Society of Biological Inorganic Chemistry, vol. 12, pp. 204-11, 2007.

[45] Lozoff B, Jimenez E, Wolf A W, "Iron-deficiency anemia and infant development: effects of extended oral iron therapy," *J. Pediatr.,* vol. 129, pp. 382-389, 1996.

[46] S. Garcia-Castineiras, "Iron, the retina and the lens: a focused review," *Exp Eye Res,* vol. 90, pp. 664-78, Jun 2010.

[47] S. Yoshida, A. Ektessabi, and S. Fujisawa, "XAFS spectroscopy of a single neuron from a patient with Parkinson's disease," *Journal of Synchrotron Radiation,* vol. 8, pp. 998-1000, 2001.

[48] Ben-Shachar D, Zuk R, Glinka Y, "Dopamine neurotoxicity: Inhibition of mitochondrial respiration," *J Neurochem,* vol. 64, pp. 718-723, 1995.

[49] E. V. Stelmashook, N. K. Isaev, E. E. Genrikhs, G. A. Amelkina, L. G. Khaspekov, V. G. Skrebitsky, *et al.*, "Role of zinc and copper ions in the pathogenetic mechanisms of Alzheimer's and Parkinson's diseases," *Biochemistry (Mosc),* vol. 79, pp. 391-6, 2014.

[50] K. Tieu, "A guide to neurotoxic animal models of Parkinson's disease.," *Cold Spring Harb. Perspect. Med.,* vol. 1, pp. 1-20, 2011.

[51] R. Betarbet, Sherer, T.B., MacKenzie, G., Garcia-Osuna, M., Panov, A.V., and and J. T. Greenamyre, "Chronic systemic pesticide exposure reproduces features of Parkinson's disease.," *Nat.Neurosci. ,* vol. 3, pp. 1301-1306, 2000.

[52] S. M. Fleming, Zhu, C., Fernagut, P.-O., Mehta, A., DiCarlo ,C.D., Seaman, R.L. , "Behavioral and immuno histochemical effects of chronic intravenous and sub cutaneous infusions of varying doses of rotenone. ," *Exp.Neurol.,* vol. 187, pp. 418-429, 2004.

[53] R. Nistico, B. Mehadawy, S. Piccirilli, N. Mercuri, "Paraquat and Rotenone induced models of Parkinson's disease.," *Journal, International Immunopathology, O. F.,* vol. 24, pp. 315-324, 2011.

[54] K. Ossowska, M. Smialowska, K. Kuter, J. Wieronska, B. Zieba, J. Wardas, *et al.*, "Degeneration of dopaminergic mesocortical neurons and activation of compensatory processes induced by a long-term paraquat administration in rats: implications for Parkinson's disease," *Neuroscience,* vol. 141, pp. 2155-65, 2006.

[55] V. N. Uversky, "Neurotoxicant-induced animal models of Parkinson's disease: understanding the role of rotenone, maneb and paraquat in neurodegeneration," *Cell and tissue research,* vol. 318, pp. 225-41, 2004.

[56] Burk RF, Lawrence RA, Lane JM, "Liver necrosis and lipid peroxidation in the rat as result of paraquat and diquat administration. Effect of selenium deficiency.," *Journal of Clinical Investigation,* vol. 65, pp. 1024-1031, 1980.

[57] C. M. Tanner, F. Kamel, G. W. Ross, J. a. Hoppin, S. M. Goldman, M. Korell, *et al.*, "Rotenone, paraquat, and Parkinson's disease," *Environmental health perspectives,* vol. 119, pp. 866-72, 2011.

[58] J. Doe. (2012, Fev). *SEA6000VX*. Available: http://www.alternatesystems.com/xrf/portfolio/sea-6000-vx/

[59] A. C. Cristovao, S. Guhathakurta, E. Bok, G. Je, S. D. Yoo, D. H. Choi, *et al.*, "NADPH oxidase 1 mediates alpha-synucleinopathy in Parkinson's disease," *J Neurosci,* vol. 32, pp. 14465-77, 2012.

[60] George Paxinos, Charles Watson, *The rat brain in stereotaxic coordinates.*, Fourth Edition ed.: Academic Press, 1998.

[61] W. M. Caudle, J. R. Richardson, K. C. Delea, T. S. Guillot, M. Wang, K. D. Pennell, *et al.*, "Polychlorinated biphenyl-induced reduction of dopamine transporter expression as a precursor to Parkinson's disease-associated dopamine toxicity," *Toxicol Sci,* vol. 92, pp. 490-9, 2006.

[62] P. Marambaud, U. Dreses-Werringloer, and V. Vingtdeux, "Calcium signaling in neurodegeneration," *Mol Neurodegener,* vol. 4, pp. 1-15, 2009.

[63] H. J. Heusinkveld, M. van den Berg, and R. H. Westerink, "In vitro dopaminergic neurotoxicity of pesticides: a link with neurodegeneration?," *Vet Q,* vol. 34, pp. 120-31, 2014.

[64] Y. Lang, D. Gong, and Y. Fan, "Calcium channel blocker use and risk of Parkinson's disease: a meta-analysis," *Pharmacoepidemiol Drug Saf,* 2015.

[65] G. Navarro, D. O. Borroto-Escuela, K. Fuxe, and R. Franco, "Purinergic signaling in Parkinson's disease. Relevance for treatment," *Neuropharmacology,* 2015.

[66] L. Forsleff, "Evidence of Functional Zinc Deficiency in Parkinson's Disease," *The Journal of Alternative and Complementary Medicine* vol. 5, pp. 57-64, 1999.